Electronic Supplementary Material (ESI) for Journal of Materials Chemistry A.

Supplementary Information

$Na_2Fe_2OS_2$, a new earth abundant oxysulphide cathode material for Na-ion batteries

Jacinthe Gamon[1,*] & Arnaud J. Perez[1,*], Leanne A. H. Jones[2,3], Marco Zanella[1], Luke M. Daniels[1], Rhun E. Morris[1], Chiu C. Tang[4], Tim D. Veal[2,3], Laurence J. Hardwick[1,2], Matthew S. Dyer[1], John B. Claridge[1] and Matthew J. Rosseinsky[1,‖]

[1]Department of Chemistry, University of Liverpool, Crown Street, Liverpool, L69 7ZD, United Kingdom

[2]Stephenson Institute for Renewable Energy, University of Liverpool, Chadwick Building, Peach Street, Liverpool, L69 7ZF, United Kingdom

[3]Department of Physics, University of Liverpool, Oliver Lodge Laboratory, Oxford Street, Liverpool L69 7ZE, United Kingdom

[4]Diamond Light Source Ltd, Harwell Science and Innovation Campus, Didcot, OX11 0DE, United Kingdom

* These authors contributed equally to the work.

‖ Corresponding author: rossein@liverpool.ac.uk

Content

1. $Na_2Fe_2OS_2$ synthesized via solid state route ($Na_2Fe_2OS_2$-SS)

1.1. Structure

A Rietveld refinement was performed, by using the structural model found for analogous $Na_2Fe_2OSe_2$, in which selenium atoms were swapped with sulphur atoms. This model fit well with our data and details and the outcome of the refinement can be found in Table S1 and S2. For the sake of realism, all uncertainties were multiplied by Berar's factor for all refinements (equal to 4.2 according to FullProf).[1] During the final stage of the fit, the composition of the main phase refined to $Na_{1.98(2)}Fe_{1.94(2)}S_{2.00(2)}O$. Because the site occupancy factors (*sof*) of Na and S refined to 1 within error, these were fixed as 1 and the final composition of $Na_2Fe_2OS_2$-SS written as $Na_2Fe_{1.94(2)}S_2O$. When refined as anisotropic, a strong difference between atomic displacement parameters (*adp*) B_{11}, B_{22} and B_{33} of Fe could be found along with a drop in the conventional reliability factors (χ^2 *de*creased from 18.8 to 16.8) and a reduced residual density in the Fourier difference map around the Fe site. However, for other atoms, this was not the case which supported the use of isotropic *adp* for modelling displacements for Na, S and O. An alternative refinement, where Fe is split into two sites along the c axis and half occupied did not lead to an improved fit. In order to validate this model comprising Fe deficiencies, *sof* of Na, Fe and S were fixed to their ideal value of 1, while maintaining other parameters fixed. The conventional reliability factors increased from 3.97 and 16.8 to 4.41 and 17.4 for R_{bragg} and χ^2 respectively. Also, the combined refinement of *adp*, with *sof* fixed to 1, led to a negative value for the *adp* of S and O (-0.03 and -0.16 respectively), indicating the need for stronger electron density on these sites (or lower on the other sites). These results indicated the presence of Fe vacancies up to 3(1) %, which could be explained by the presence of partially oxidized iron into Fe^{3+}, or a p-type doping.

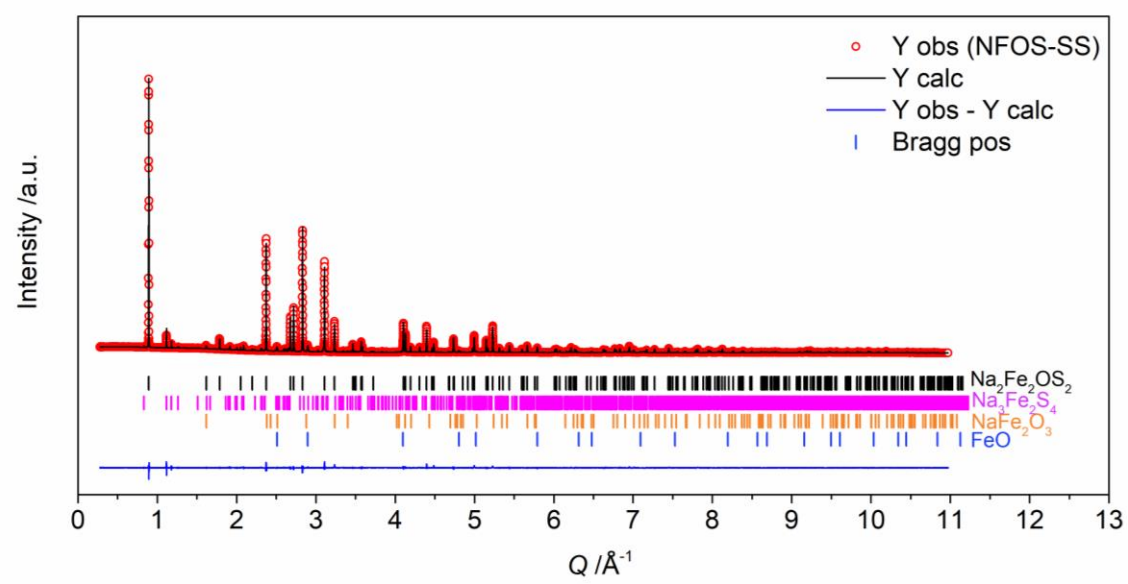

Figure S1. Final Rietveld refinement of the synchrotron X-ray diffraction pattern of $Na_2Fe_2OS_2$ (Diamond light source, I11 beam line, λ = 0.824605 Å) prepared by solid-state route ($Na_2Fe_2OS_2$-SS) with I_{obs} (red dots), I_{calc} (black line), I_{obs}-I_{calc} (blue line), and Bragg reflections (black tick marks for $Na_2Fe_2OS_2$, pink tick marks for $Na_3Fe_2S_4$, orange tick marks $NaFe_2O_3$ and blue tick marks for FeO).

Table S1. Result of the Rietveld refinement of $Na_2Fe_2OS_2$ prepared by solid state reaction route ($Na_2Fe_2OS_2$-SS)

Identifier	**$Na_2Fe_2OS_2$-SS**
Radiation	**SXRD**
Empirical formula	$Na_2Fe_{1.94(2)}S_2O$
Formula weight (g·mol^{-1})	237.8
Space group	*I*4/*mmm*
Z	2
Density (g·cm^{-3})	3.412
Temperature (K)	298
Wavelength (Å)	0.824605
d spacing range (Å)	0.5726 – 22.6275
2θ (°) range	2.0840 - 92.1120
2θ (°) step	0.004
No. of reflections	240
No. of refined parameters	19
***a* (Å)**	4.04222(1)
***c* (Å)**	14.07319(9)
Volume (Å^3)	229.950(2)
R_p	10.6
R_{wp}	9.89
R_{exp}	2.29
R_{Bragg}	4.29
χ^2	18.7
$\rho_{min./max.}$ **residuals (e$^-$·Å^{-3})**	[-0.85 / +1.63]

Table S2. Atomic positions, isotropic (B_{iso}), anisotropic (B_{11}, B_{22}, B_{33}) and equivalent (B_{eq}) atomic displacement parameters, and site occupancy factor (*sof*) for $Na_2Fe_2OS_2$, $Na_2Fe_2OS_2$-SS.

Site	**Wyckoff position**	**x**	**y**	**z**	***sof***	$\boldsymbol{B_{iso}}$ **/** $\boldsymbol{B_{11}}$**,** $\boldsymbol{B_{22}}$**,** $\boldsymbol{B_{33}}$**,** $\boldsymbol{B_{eq}}$ **(Å²)**
Na	4*e*	0	0	0.1764(2)	1	0.71(8)
Fe	4*c*	0	0.5	0	0.972(8)	0.0(3), 0.00(1), 0.48(3), 0.32(6)
S	4*e*	0	0	0.3774(2)	1	0.10(4)
O	2*a*	0	0	0	1	0.2(2)

1.2. Improving purity of the $Na_2Fe_2OS_2$ phase: solid state synthesis attempts

In order to improve the purity of the sample, different synthesis conditions such as temperature, quenching procedure, the use of different precursors, of oxygen getters, as well as slight deviation from stoichiometry were varied. Unfortunately, none of these conditions improved the purity of the sample. The results are summarized below.

1.2.1. Reaction time

The first step of the synthesis reaction at 500 °C was maintained for 20 hours, whereas the annealing time at 600 °C during the second step was varied (3, 6 and 12 hours). Impurities present after 3 h reaction are $Na_3Fe_2S_4$ and $NaFeO_2$ (Figure S2, bottom). After 6 hours, the amount of these impurity phases decreases slightly compared to the main $Na_2Fe_2OS_2$ phase, and a new impurity of FeO can be observed (Figure S2, middle). After 12 hours, the amount of FeO greatly increased, while $Na_3Fe_2S_4$ impurity remains, with a slight increase of the peak intensity (Figure S2, top). These results suggest that the $Na_2Fe_2OS_2$ phase is unstable at 600 °C and decomposes to $Na_3Fe_2S_4$ and FeO.

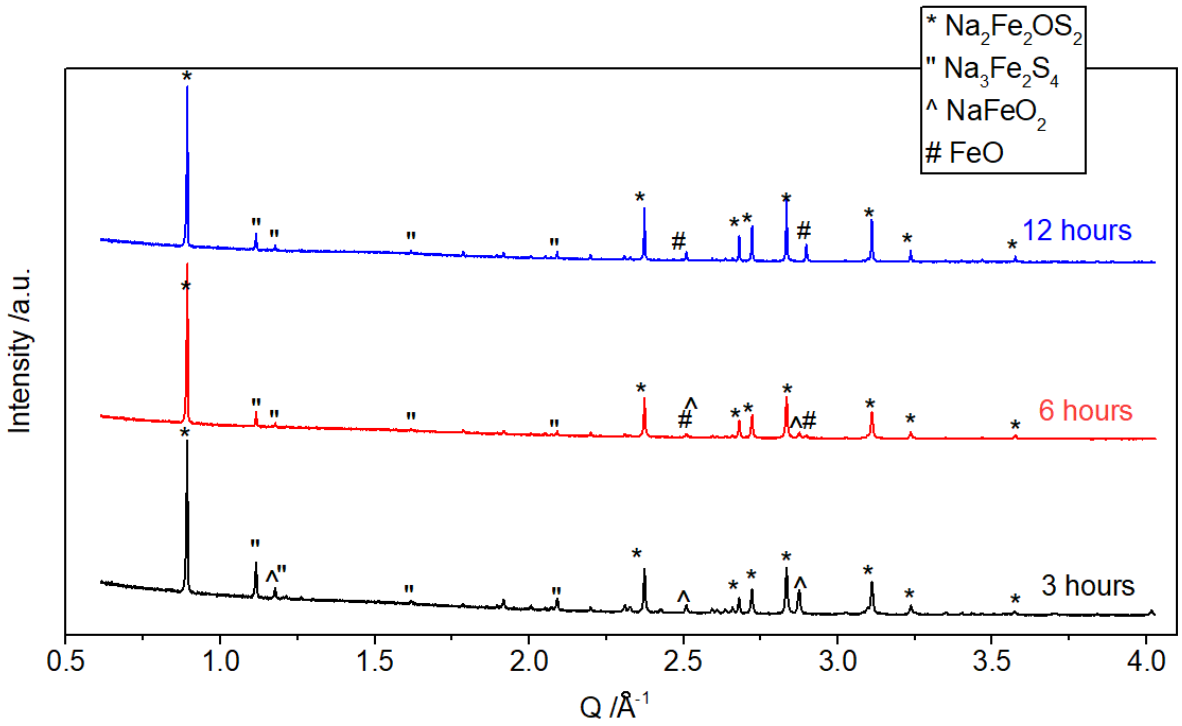

Figure S2. XRD patterns of samples prepared using Na metal, Fe_2O_3, FeS and S, reacted at 500 °C for 20 hours, reground and reannealed at 600 °C for different amount of times (in legend). λ = 1.5406 Å.

1.2.2. Reaction temperature

A synthesis using a lower temperature of 550 °C resulted in a less pure sample, with hardly any $Na_2Fe_2OS_2$ phase (Figure S3, bottom). As such, in an attempt to stabilize the kinetic phase, as opposed to the thermodynamic phases $Na_3Fe_2S_4$ and FeO, the annealing temperature was increased to 700 °C and 900 °C, the sample was left at this temperature for 1 hour and the reaction was then quenched in ice water. At these temperatures, the precursor mixture melted and the phase $Na_2Fe_2OS_2$ was not identified in the sample (Figure S3, top). These results suggest that an optimal temperature of 600 °C is needed to favor the growth of the desired phase while preventing its decomposition. Moreover, quenching the reaction from 600 °C after 12 hours of reaction, does not improve the purity of the sample, suggesting that the decomposition occurred during the annealing step.

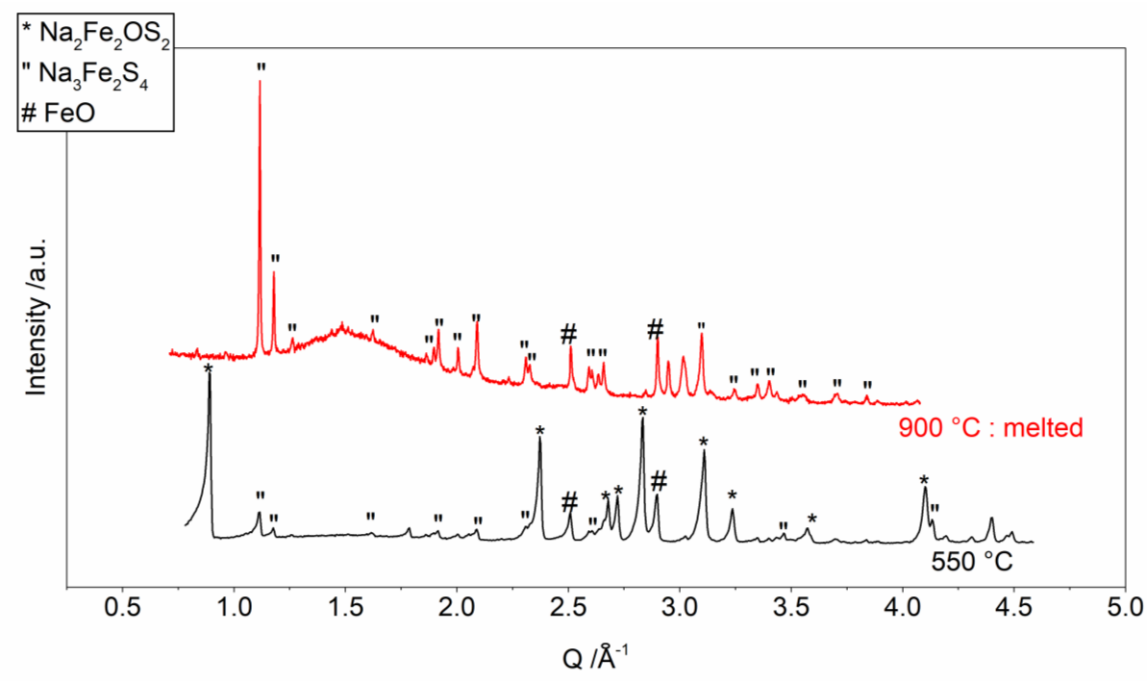

Figure S3. XRD patterns of samples reacted at different temperature for 6 hours λ = 1.5406 Å (red curve) λ = 0.709032 Å (black curve).

1.2.3. Different precursors

After the first step at 500 °C, phases present are $Na_3Fe_2S_4$, Na_2S, FeS, Fe_3O_4 and $NaFeO_2$. Other precursors were then considered in order to stabilize the kinetic phase $Na_2Fe_2OS_2$. Na_2S, FeS, Fe_2O_3 and Fe on the one hand and Na_2O and FeS on the other hand, where Na and Fe are already in the same oxidation state as in $Na_2Fe_2OS_2$, where used. After reacting at 600 °C for 6 hours, the amount of FeO and $Na_3Fe_2S_4$ impurity was higher than when Na metal and Fe_2O_3 precursors were used (Figure S4).

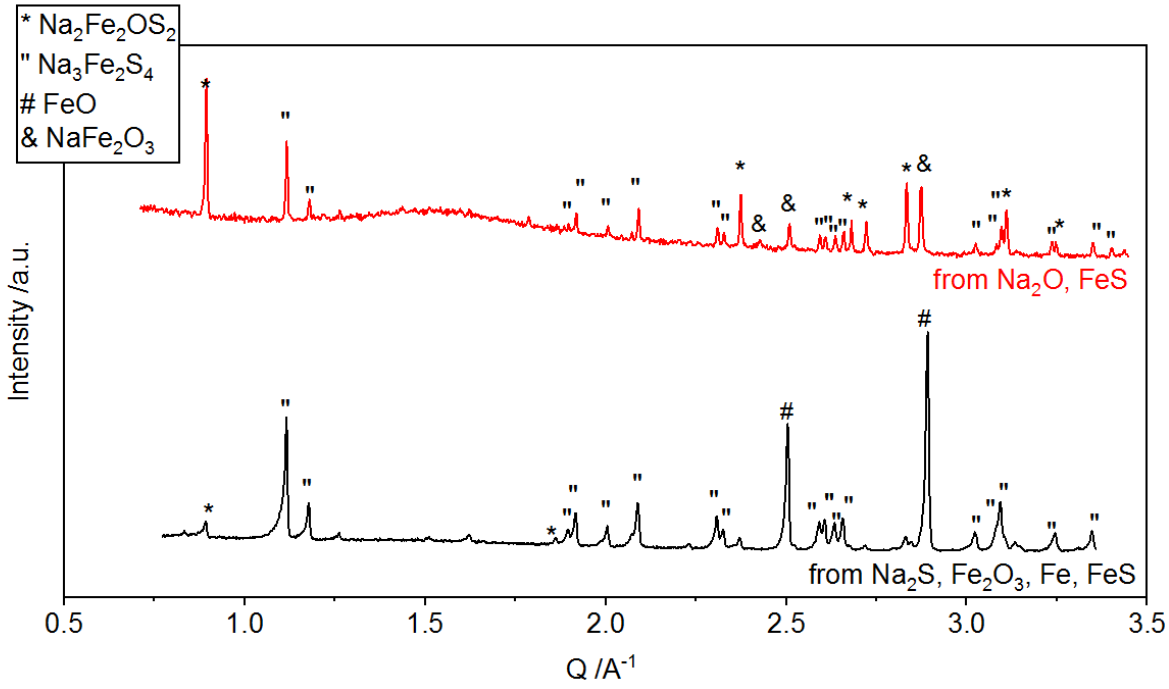

Figure S4. XRD patterns of samples reacted with different precursors at 600 °C for 6 hours λ = 1.5406 Å (red curve) λ = 0.709032 Å (black curve).

1.2.4. Deviation from stoichiometry

Slight deviations from stoichiometry were considered. Indeed, as the composition of the sample refined to a slightly defective Fe content, the charge balance can be explained by the presence of some Fe^{3+} thermodynamically stabilized. Therefore, samples containing either Fe or Na deficiency were prepared, with composition $Na_2Fe_{1.9}OS_2$ and $Na_{1.8}Fe_2OS_2$. Also, from the Rietveld refinement, the sum of the impurities $Na_3Fe_2S_4$ and FeO leads to the stoichiometry $Na_{1.5}Fe_{2.01}S_{2.03}O$, which suggest that excess Na would be needed to obtain the desired stoichiometry of $Na_2Fe_2OS_2$. Na metal was then added in excess (3 % mass excess). None of these attempts were successful.

2. $Na_2Fe_2OS_2$ synthesized via solid mechanosynthesis ($Na_2Fe_2OS_2$-MW)

2.1. Optimization of the mechanosynthesis procedure

We have used this method for the synthesis of $Na_2Fe_2OS_2$ by ball milling Na_2O and FeS in an Argon containing grinding bowl. First, a sample having the exact stoichiometry of the desired phase was tried. The XRD pattern of this phase is shown in Figure S6a, and a Rietveld fit of the phase enabled to approximate the amount of each impurities (Figure S5).

$$100\ Na_2Fe_2OS_2 \Leftrightarrow 40\ Na_2Fe_2OS_2 + 5\ Na_3Fe_2S_4 + 43\ FeO + 11\ Fe$$

The grinding time did not influence the amount of these impurities. In order to shift the reaction to the left, changes in the precursor ratio were performed. The quantification of the ratio of the different phases suggest that most of the impurities are Fe and O rich. Therefore, an excess of Na and S was introduced thanks to the addition of Na_2S precursor. Its solubility in many solvents will enable the removal of the excess Na_2S after reaction. For a starting precursor ratio of 1 Na_2O + 2 FeS + 0.75 Na_2S (composition $Na_{3.5}Fe_2S_{2.75}O$), the mechanosynthesized sample contained the crystalline phases $Na_2Fe_2OS_2$ and FeO, where the amount of FeO was considerably reduced compared to the sample prepared with the ideal stoichiometry (Figure S6b). As the excess Na_2S could not be seen in the diffraction pattern, we concluded that it was amorphised during the ball milling step. Any greater excess Na_2S led to the formation of a sulphide phase Na_6FeS_4. To remove the FeO impurity, samples were made at compositions calculated by: $Na_{3.5}Fe_2S_{2.75}O - x$ FeO. For x = 0.1 ($Na_{3.5}Fe_{1.9}S_{2.75}O_{0.9}$), no FeO crystalline impurity was found in the sample after reaction (Figure S6c). However, according to the Rietveld fit of the resulting phase, a small

amount of Fe metal impurity remained (Figure S5). The balanced chemical equation is:

$$Na_{3.5}Fe_{1.9}O_{0.9}S_{2.75} \rightarrow 0.9\ Na_2Fe_2OS_2 + [0.1\ Fe^{2+} + 1.7\ Na^{+} + 0.95\ S^{2-}]$$

$$Na_{3.5}Fe_{1.9}O_{0.9}S_{2.75} \rightarrow 0.9\ Na_2Fe_2OS_2 + [0.1\ Fe^{2+} + 0.1\ S^{2-}] + 0.85\ Na_2S$$

$$Na_{3.5}Fe_{1.9}O_{0.9}S_{2.75} \rightarrow 0.9\ Na_2Fe_2OS_2 + 0.1\ Fe^{0} + 0.85\ Na_2S_{1.1}$$

The amount of Fe metal impurity was quantified by Rietveld analysis. The mass ratio of $Na_2Fe_2OS_2$ and Fe phases was: 96.26/3.74, which corresponds to a mole ratio 86/14, close to that calculated in the balanced chemical equation of the reaction.

In order to remove the excess Na_2S_x species, the sample was washed in methanol. Because of the relatively low solubility of Na_2S in methanol, the washing procedure was repeated 6 times to ensure its complete removal. The mechanosynthesized samples before and after washing are named $Na_2Fe_2OS_2$-M and $Na_2Fe_2OS_2$-MW respectively. A portion of the washing solution was then dried (by bringing the solution to boil under an N_2 gas flow, followed by drying under vacuum). XRD of the dried methanol washing solution confirmed that the phase removed is Na_2S (Figure S7), and XPS analysis performed before and after washing the material shows a large decrease of the Na_2S contribution in the S 2*p* peaks region ($2p_{3/2}$ peak at 161.5 eV in Figure S8) so that the sulphur peak from the material ($2p_{3/2}$ peak at 162.2 eV) can be observed after washing. The outcome and mass balance of the washing procedure as well as the elemental analysis of the resulting powders is presented in Table S4. According to the chemical equation, the amount of Na_2S_x to be washed corresponds to 24 wt% of the total mass. The amount of powder remaining after the washing procedure corresponds to 78(1) % of the initial mass of powder before

washing. The efficiency of the washing procedure was therefore calculated to be 22(1)/24 = 92(4) %.

In an attempt to improve the crystallinity of the compound prepared by mechanosynthesis, $Na_2Fe_2OS_2$-M and $Na_2Fe_2OS_2$-MW samples were annealed in a sealed tube at 400°C and 600 °C for 6 hours. This resulted in the partial decomposition of the phase with the crystallization of $Na_3Fe_2S_4$ in particular. Additionally, a sample with the same initial composition (excess Na_2S) was prepared via solid state route with an annealing step at 600 °C for 6 hours. This reaction resulted in a mixed phase compound, with low amount of the desired phase. These results further confirm the metastability of $Na_2Fe_2OS_2$ at elevated temperature.

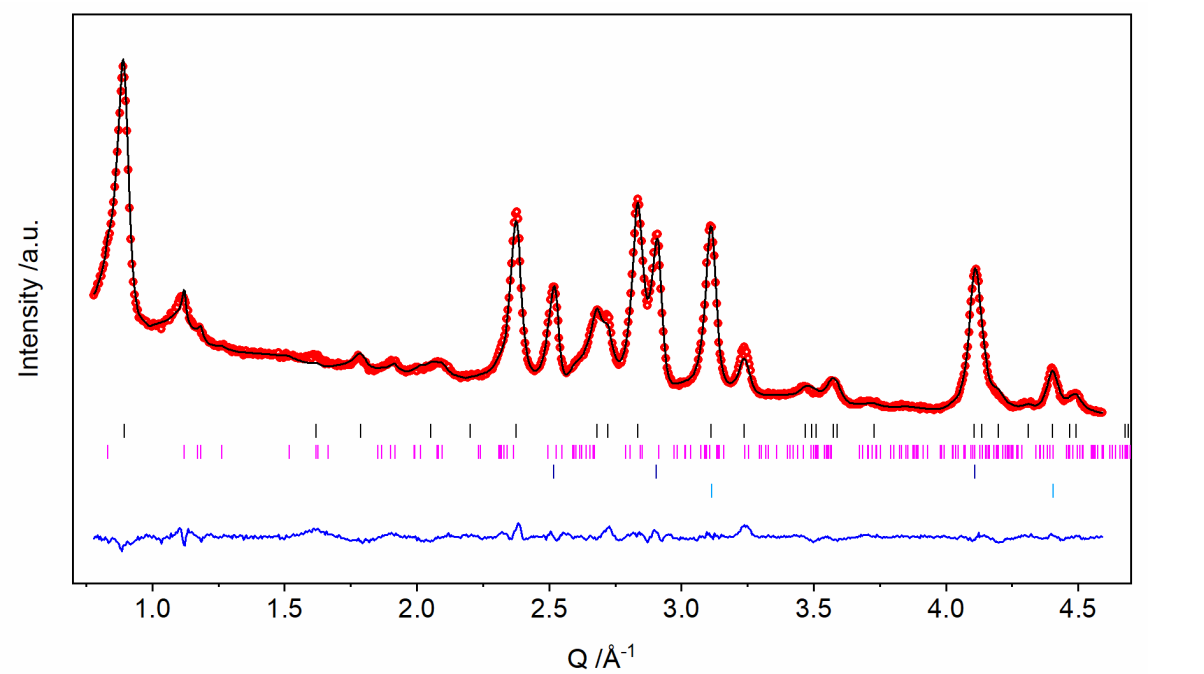

Figure S5. Rietveld refinement of the laboratory X-ray diffraction pattern of $Na_2Fe_2OS_2$ made by mechanosynthesis from Na_2O and FeS in a 1:2 molar ratio, with I_{obs} (red dots), I_{calc} (black line), I_{obs}-I_{calc} (blue line), and Bragg reflections (black tick marks for $Na_2Fe_2OS_2$, pink tick marks for $Na_3Fe_2S_4$, blue tick marks for FeO, and light blue tick marks for Fe metal).

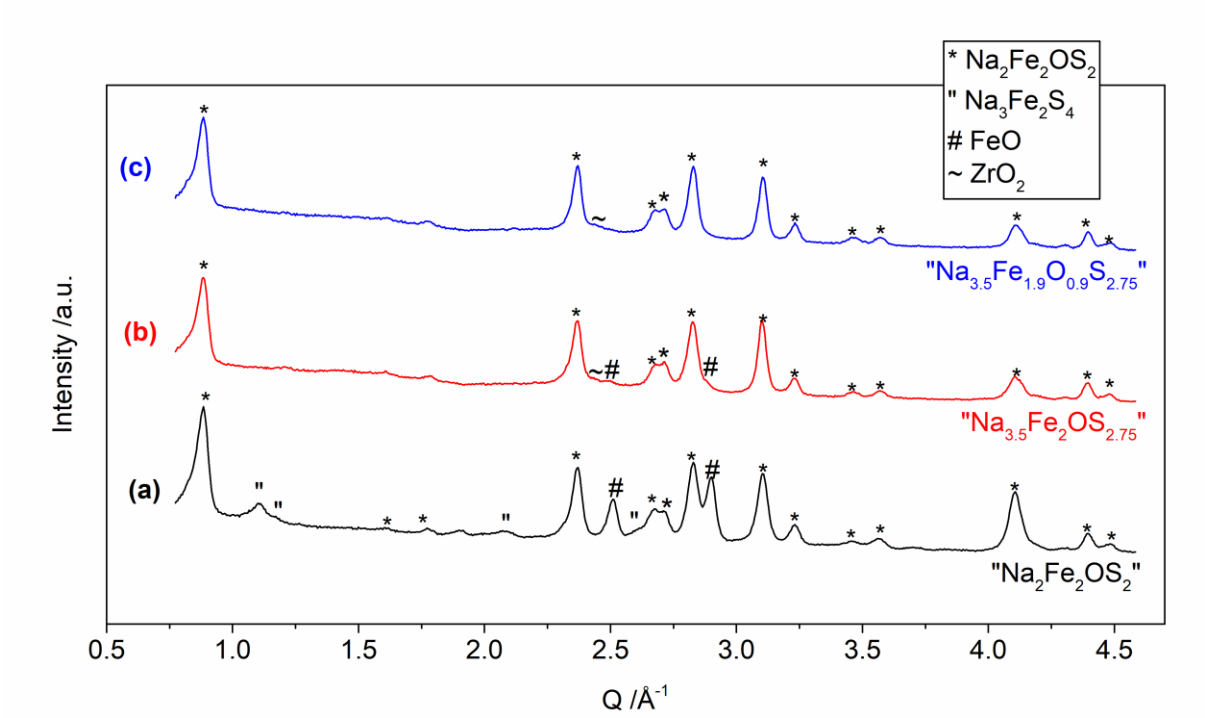

Figure S6. XRD patterns of samples made by mechanosynthesis under Ar, using Na_2O, FeS and Na_2S as precursors (stoichiometry in legend). λ = 0.70932 Å.

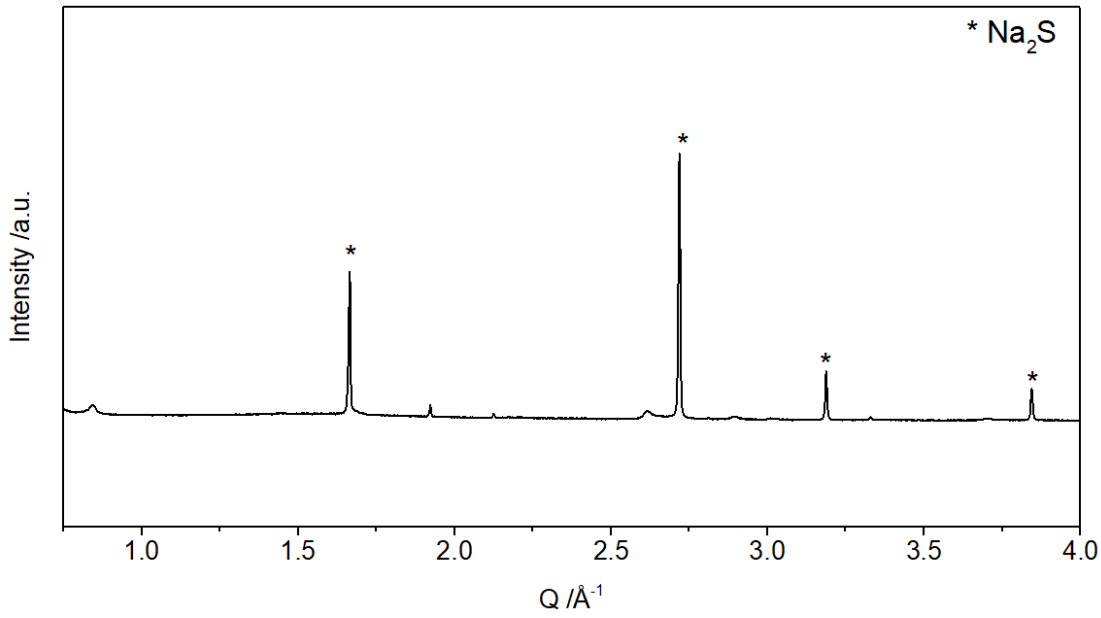

Figure S7. XRD pattern of the powder dissolved in methanol during the washing procedure. λ = 1.5406 Å.

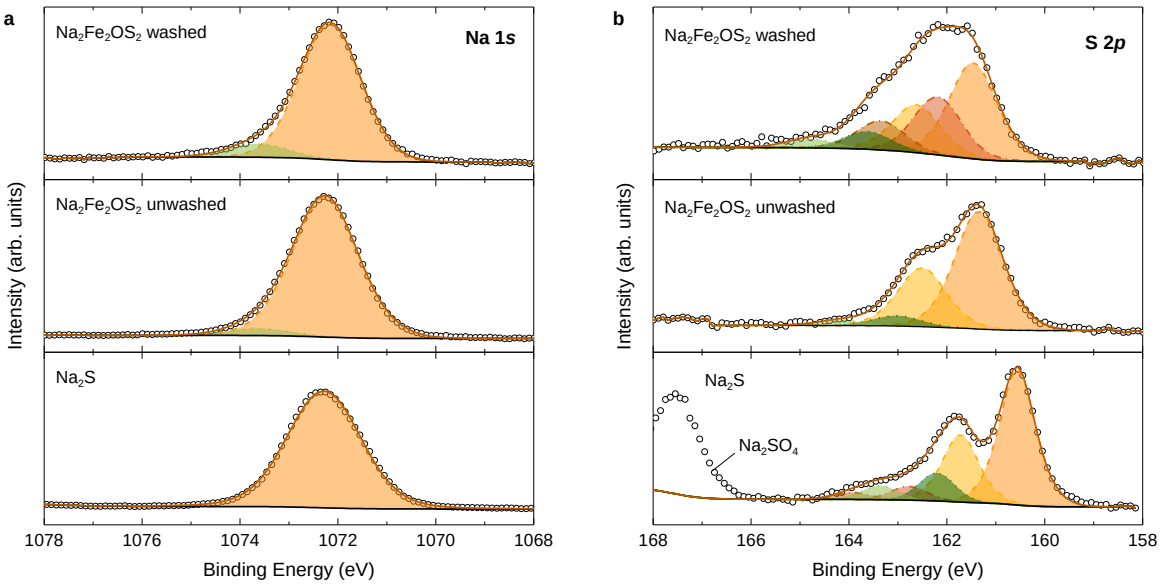

Figure S8. XPS analysis of the pristine sample before and after methanol washing. (a) The Na 1*s* spectra shows little variation between the different samples, including with the reference sample Na_2S. (b) The S 2p spectra shows one main doublet (S $2p_{3/2}$ peak at 160.9 eV) for the unwashed sample that can be ascribed to the excess Na_2S on the surface. Na_2S is measured as a reference, with some Na_2SO_4 impurity. The $Na_2Fe_2OS_2$ sample washed in methanol shows a new doublet at higher binding energy ($2p_{3/2}$ peak at 162.2 eV) that we attribute to sulphur atoms in the $Na_2Fe_2OS_2$ phase. Sulphur atoms bonding to iron have a higher binding energy than sulphur atoms bonded only to sodium due to the higher electronegativity of iron compared to sodium.

2.2. Composition and microstructure

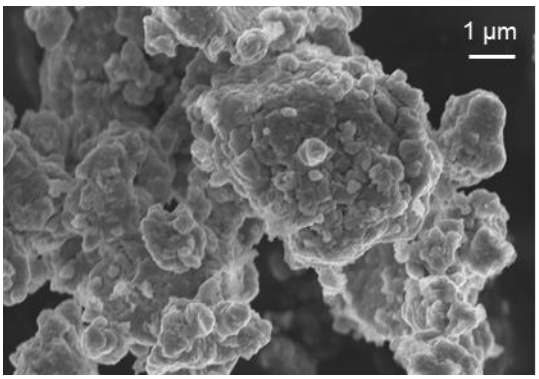

Figure S9. SEM picture of $Na_2Fe_2OS_2$ synthesized through mechanosynthesis

2.2.1. Le Bail fitting of the mechanosynthesized sample $Na_2Fe_2OS_2$-MW

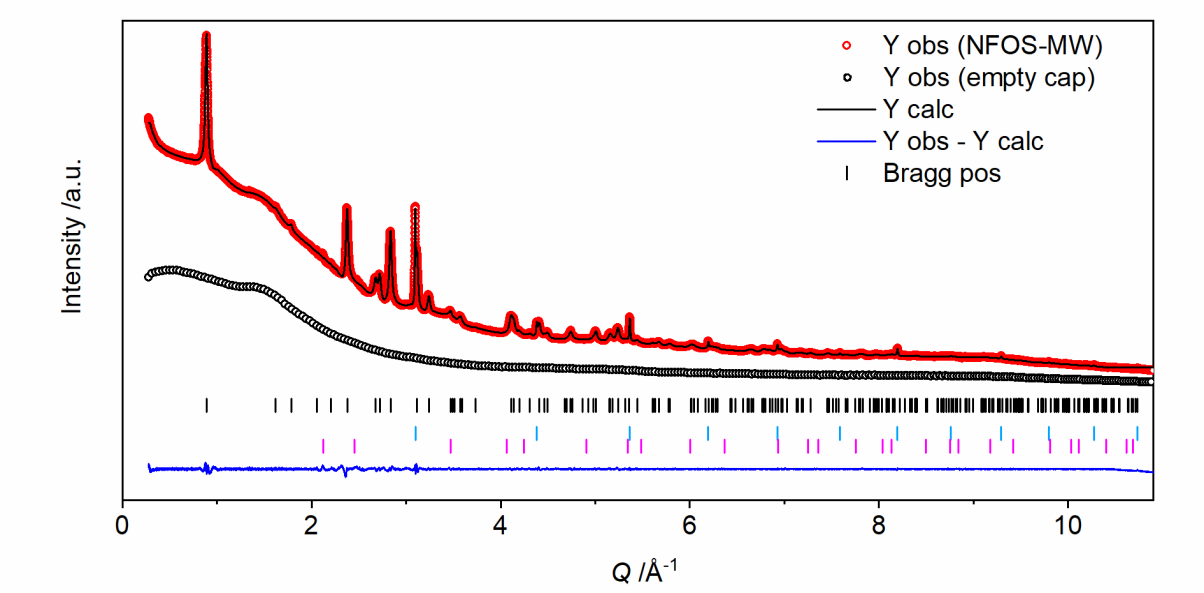

Figure S10. Le Bail fit of the $Na_2Fe_2OS_2$ phase, prepared by mechanosynthesis after methanol washing ($Na_2Fe_2OS_2$-MW), in the *I*4/*mmm* space group with lattice parameters *a* = 4.0325(1) Å and *c* = 14.077(1) Å (Diamond light source, I11 beam line) with I_{obs} (red dots), I_{calc} (black line), I_{obs}-I_{calc} (blue line), and Bragg reflections (black tick marks for $Na_2Fe_2OS_2$, blue tick marks for Fe, pink tick marks for ZrO_2). Comparison of the diffraction pattern of $Na_2Fe_2OS_2$-MW and of an empty capillary, showing the contribution of the capillary to the background.

2.2.2. Determination of the amount of amorphous content in $Na_2Fe_2OS_2$-MW

The amount of amorphous content was determined by using the quantitative phase analysis method described in the literature.[2–4] This method consists of mixing a known amount of the $Na_2Fe_2OS_2$ phase with an internal standard of similar absorption coefficient and comparing the relative weight percent weighed initially with that calculated by the program. The relative weight fraction of amorphous phase in the sample, w_A, can be derived from the equation:

$$w_A = \frac{w_{R,calc} - w_{R,mes}}{w_{R,calc} - w_{R,mes} * (1 - w_{NFOS,calc})}$$

where $w_{R,calc}$ and $w_{NFOS,calc}$ are the weight fraction of the reference ($Na_3Fe_2S_4$) and $Na_2Fe_2OS_2$, respectively, to the total amount of crystalline powder calculated by Rietveld analysis, $w_{R,mes}$ is the weight fraction of the reference to the total mass of

powder weighed experimentally. We have $w_{R,mes} + w_{NFOS,mes} = 1$, and by taking the amount of Fe impurity into account, we have the relations: $w_{R,calc} + w_{NFOS,calc} + w_{Fe,calc} = 1$.

The reference sample $Na_3Fe_2S_4$ was prepared by solid state synthesis method by grinding Na_2S and FeS in stoichiometric amounts in an agate mortar, and heating the mixture in an alumina crucible inside a quartz tube sealed under vacuum at 600 °C for 12 hours (with cooling and heating ramp rates of 5 °C·min^{-1}). In order to get an accurate value of calculated weight fraction, the values of the Brindley coefficient for the different phases need to be determined. This parameter accounts for microabsorption effects that become non-negligible when the difference in linear absorption coefficient and particle size is different between the two phases.[5,6] Its value is tabulated in the literature and only requires knowledge of the value of (μ_j - μ)R, where μ_j is the linear absorption coefficient of phase j, μ is the mean average linear absorption coefficient of the sample ($\mu = \sum \mu_j w_{j,mes}$), and R the particle size. A strong error can be obtained on the latter, as it represents the average size of agglomerated grains, rather than the coherent scattering domain size. To determine this value for the reference material $Na_3Fe_2S_4$, a known amount of solid state synthesized $Na_2Fe_2OS_2$ ($Na_2Fe_2OS_2$-SS, which does not contain any amorphous content) and $Na_3Fe_2S_4$ were thoroughly mixed and the Brindley coefficients of both phases were varied during the Rietveld refinement of the diffraction data of these mixed phases, until the quantitative phase analysis result matched the amount weighed. A value of R = 40 µm was obtained for $Na_3Fe_2S_4$. The value of R for $Na_2Fe_2OS_2$-MW was estimated from the SEM image, while that of the Fe impurity, which is considered dispersed into the $Na_2Fe_2OS_2$ powder, was taken from the value of the coherent scattering domain size from the peak profile shape of the XRD pattern (Debye

Scherrer). Then, 51.7 mg of $Na_2Fe_2OS_2$-MW and 26.1 mg of $Na_3Fe_2S_4$ were thoroughly mixed and ground in an agate mortar for 15 min before collecting diffraction data on the mixed phases. The values of the different parameters used for the quantitative phase analysis through Rietveld refinement as well as the outcome of the analysis are reported in the table below. The errors are estimated from a maximum error on the value of *R* of 150 %.

Table S 3. Parameters used for the determination of the amorphous contribution in $Na_2Fe_2OS_2$-MW thanks to the quantitative phase analysis method.

	$Na_2Fe_2OS_2$-MW	**$Na_3Fe_2S_4$**	**Fe**
Mass weighed (mg)	51.7	26.1	(~1)
$w_{j,mes}$ (%)	66.4(5)	33.5(5)	/
μ_j (cm^{-1}, λ = 0.826 Å)	114.2	78.2	413
μ (cm^{-1})	106		
***R* (cm)**	$1 \cdot 10^{-3}$	$4 \cdot 10^{-3}$	$7 \cdot 10^{-6}$
$(\mu_j - \mu)R$	0.01	-0.11	0.00
Brindley coefficient[5,6]	0.980	1.200	1.000
$w_{j,calc}$ (%)	42(3)	55(3)	2.3(1)
w_A (%)	60(5)	/	/

2.2.3. Elemental analysis

Table S4. Result of the methanol washing procedure. $Na_2Fe_2OS_2$-M is the mechanosynthesized sample at composition $Na_{3.5}Fe_{1.9}O_{0.9}S_{2.75}$, $Na_2Fe_2OS_2$-MW is the same sample after methanol washing, and residue is the compound dissolved in the washing solution. Elemental analysis was performed by ICP-OES for Na, Fe (and S for the residue), and by CHNS for S in the powders.

Sample	Phases identified in the XRD pattern	Expected composition	Elemental analysis	Percentage of the initial total mass
$Na_2Fe_2OS_2$-M	$Na_2Fe_2OS_2$, Fe + amorphous Na_2S	Na: 3.5 Fe: 1.9 S: 2.75	Na 3.35(5) Fe 1.90(3) S 2.83(2)	100
$Na_2Fe_2OS_2$-MW	$Na_2Fe_2OS_2$, Fe (1.8(2) w%)	Na: 2 Fe: 2 S: 2	Na 2.2(1) Fe 2.00(1) S 2.29(1)	78(1)
Residue	Na_2S + amorphous peaks	Na: 2 Fe: 0 S: 1.1	Na: 2.00(2) Fe: 0.01(1) S: 0.75(1)	26(1)

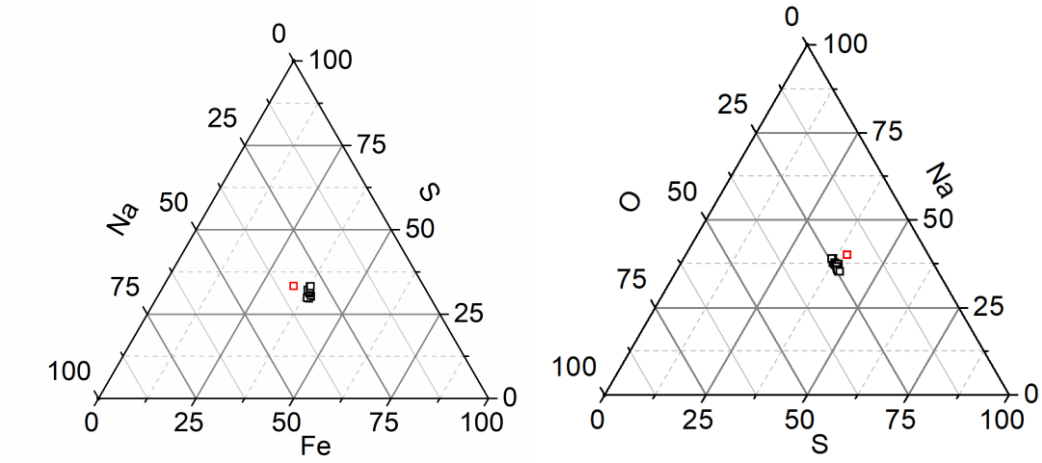

Figure S11. Elemental analysis performed by SEM-WDX on $Na_2Fe_2OS_2$-MW on 10 different spots in the powder (black points) and the expected composition $Na_2Fe_2OS_2$ (red point) showing that the composition of $Na_2Fe_2OS_2$-MW is close to the one expected and homogeneous on the micrometer scale (spot size of the WDX probe: 1-2 µm).

2.3. Structure of mechanosynthesized $Na_2Fe_2OS_2$ ($Na_2Fe_2OS_2$-MW)

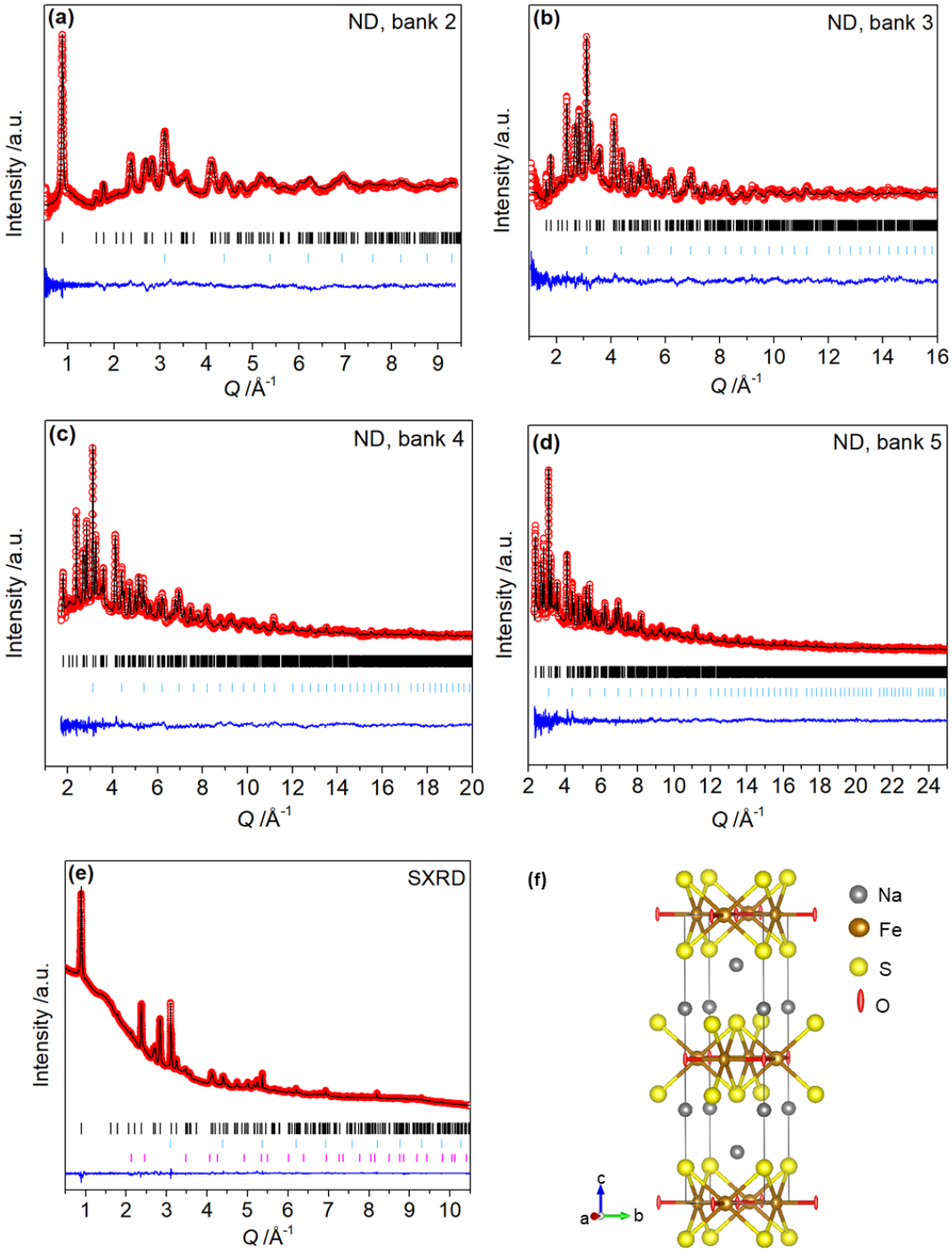

Figure S12. Final Rietveld refinement against neutron powder diffraction data (ISIS neutron source, Polaris) from (a) bank 2 (2θ = 168.330 °), (b) bank 3 (2θ = 89.580 °), (c) bank 4 (2θ = 30.000 °), (d) bank 5 (2θ = 30.000 °), and (e) against synchrotron X-ray diffraction (Diamond light source, I11 beam line) of $Na_2Fe_2OS_2$ ($Na_2Fe_2OS_2$-MW) , with I_{obs} (red dots), I_{calc} (black line), I_{obs}-I_{calc} (blue line), and Bragg reflections (black tick marks for $Na_2Fe_2OS_2$, blue tick marks for Fe, and pink tick marks for ZrO_2). Contribution of the capillary to the background of the pattern is shown in Figure S10. (f) Structure of $Na_2Fe_2OS_2$ from the refined model, with atoms shown as displacement ellipsoid with a probability of 90 %.

Table S5. Result of the Rietveld refinement of $Na_2Fe_2OS_2$ prepared by mechanosynthesis after ($Na_2Fe_2OS_2$-MW) methanol washing.

Identifier	**$Na_2Fe_2OS_2$-MW**				
Radiation	**SXRD**	**ND, bank 2**	**ND, bank 3**	**ND, bank 4**	**ND, bank 5**
Empirical formula	$Na_{1.98(4)}Fe_{1.96(4)}S_{1.98(2)}O$				
Formula weight (g·mol^{-1})	237.8				
Space group	*I4/mmm*				
Z	2				
Density (g·cm^{-3})	3.450				
Temperature (K)	298				
Wavelength (Å) Angle (°) /	0.82654(1)	25.990	52.210	92.590	146.720
d spacing range (Å)	0.5335 - 22.7255	0.5788 - 13.9828	0.2807 – 5.9297	0.1614 – 3.6944	0.1857 - 2.6986
TOF (μsec.) / 2θ (°) range	2.0840 - 92.1120	1208.0513 - 24884.8281	1107.6846 - 19936.9336	1107.3549 - 19937.9629	1103.8363 - 19944.8594
TOF (μsec.) / 2θ (°) step	0.004	7.8244	6.5131	6.5135	3.2546
No. of reflections	277	219	1632	7932	5300
No. of refined parameters	16 (profile) 16 (atomic)				
***a* (Å)**	4.0325(1)	4.0304(2)			
***c* (Å)**	14.077(1)	14.07(1)			
Volume (Å^3)	228.91(3)	228.5(2)			
R_p	12.0	14.1	20.3	20.3	20.8
R_{wp}	8.20	13.1	13.1	15.3	18.7
R_{exp}	2.80	7.23	8.78	8.65	16.19
R_{Bragg}	2.17	4.19	13.2	16.2	14.1
χ^2	8.57	3.28	2.24	3.14	1.34
$\rho_{min./max.}$ residuals (barns/e^-·Å^{-3})	[-2.7 / +2.8]	[-2.5 / +0.1]	[-1.1 / +0.1]	[-4.4 / +1.3]	[-0.3 / +0.6]

Table S6. Atomic positions, isotropic (B_{iso}), anisotropic (B_{11}, B_{22}, B_{33}) and equivalent (B_{eq}) atomic displacement parameters, and site occupancy factor (*sof*) for $Na_2Fe_2OS_2$ prepared by mechanosynthesis after methanol washing ($Na_2Fe_2OS_2$-MW) obtained from the Rietveld fit of the ND and SXRD data.

Site	**Wyckoff position**	**x**	**y**	**z**	***sof***	**B_{iso} / B_{11}, B_{22}, B_{33}, B_{eq} (Å^2)**
Na	4*e*	0	0	0.176(2)	1	1.6(3)
Fe	4*c*	0	0.5	0	0.99(2)	2.0(4), 1.0(4), 1.8(4), 2.1(5)
S	4*e*	0	0	0.376(3)	0.96(4)	2.3(5)
O	2*a*	0	0	0	0.98(1)	0.1(2), 0.1(2), 1.6(9), 1.2(5)

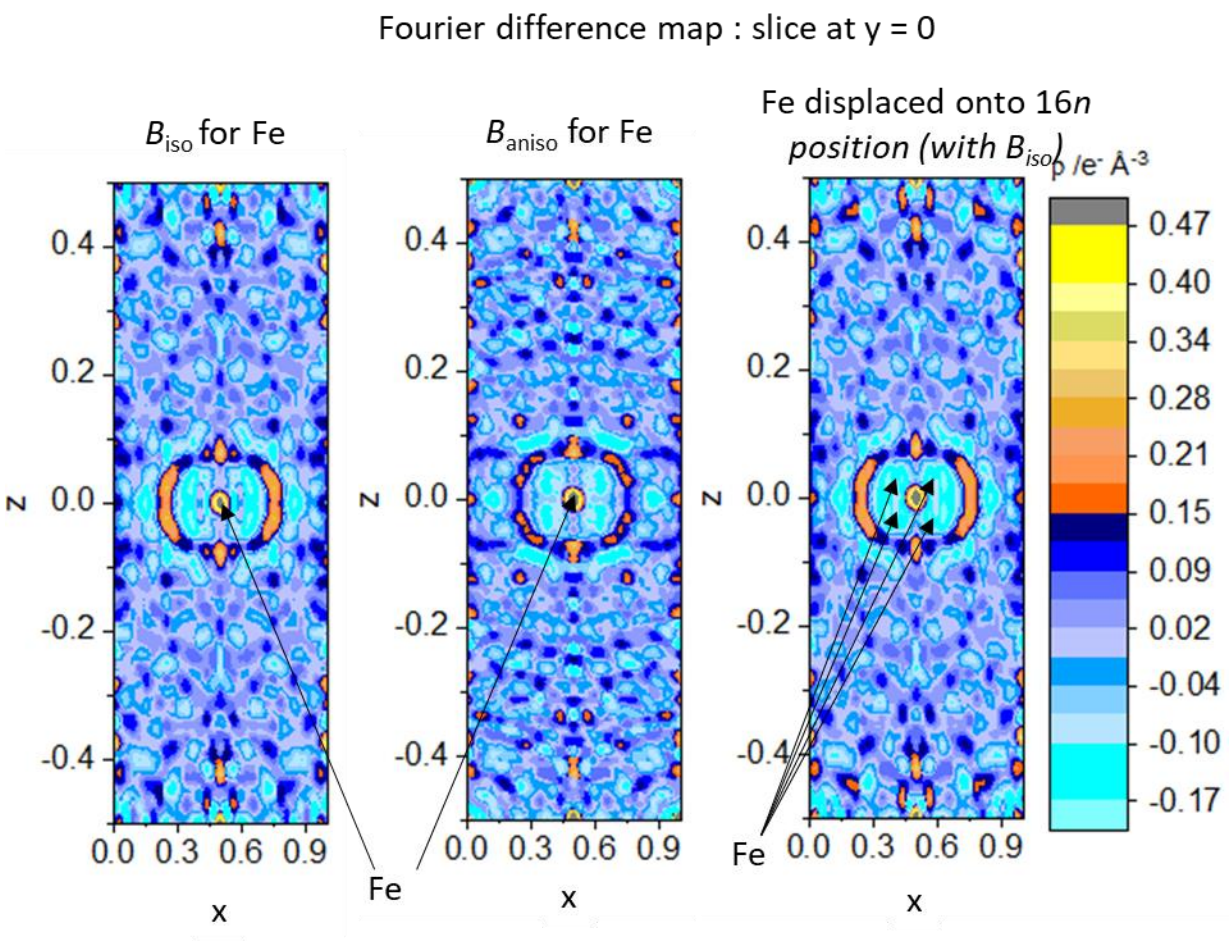

Figure S13. Fourier difference map of $Na_2Fe_2OS_2$ ($Na_2Fe_2OS_2$-MW) diffraction data from neutron bank 5 using different model, with isotropic (B_{iso}) or anisotropic (B_{aniso}) atomic displacement parameters, showing the reduced residual density around the Fe atom when it is in 4*c* position using B_{aniso} to model its displacement. The Fourier difference map shows that there is more residual electron density around Fe when it is split on a 16*n* position, moreover, this model does not match better the distances obtained from the EXAFS measurement, and was therefore not selected.

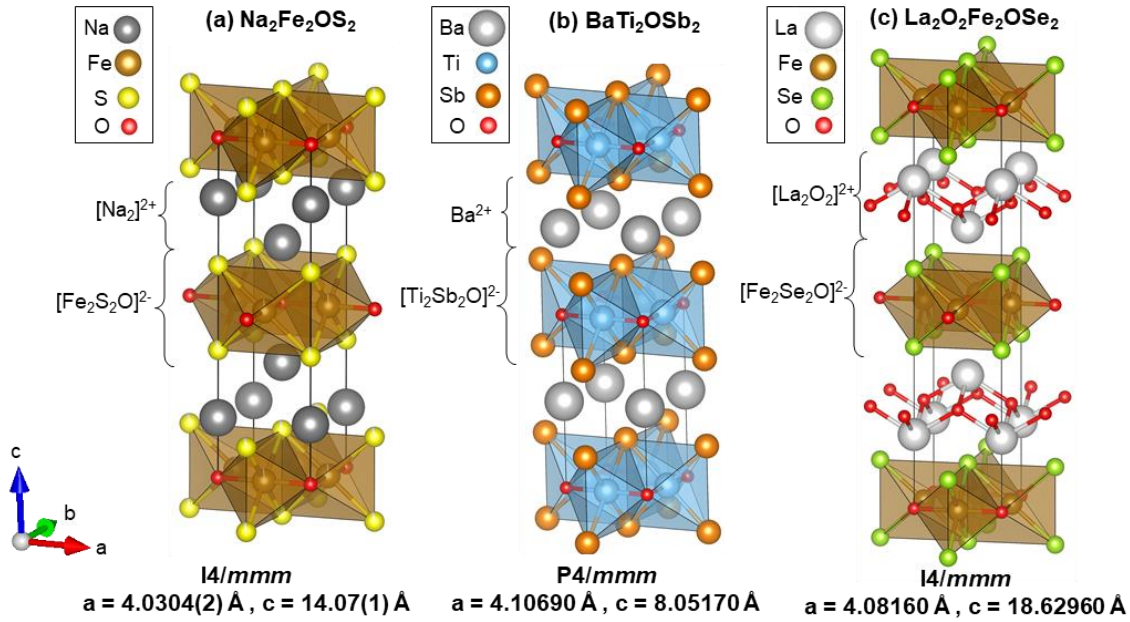

Figure S14. (a) $Na_2Fe_2OS_2$ structure showing the Fe_2O anti-CuO_2 type layer and comparison with the structures of $BaTi_2OSb_2$ (b) and $La_2O_2Fe_2OSe_2$ (c), showing the $[M_2OQ_2]^{2-}$ (M = Fe, Ti; Q = S, Se, Sb) type layer alternating with a 2+ charged layer of different type.

2.4. Infrared spectroscopy

Table S 7. Assignment of peaks in the FTIR spectra of the $Na_2Fe_2OS_2$ samples presented in Figure 1 and 3. Samples synthesized under Ar, synthesized under dry air and stored in dry air show the same features that we therefore assigned to the material. The sample prepared by the solid-state method shows similar peaks as well as contributions from $Na_3Fe_2S_4$. The sample stored in humid air mostly shows contributions from Na_2CO_3, H_2O, OH bonds as well as other unidentified features that could correspond to Fe-based decomposition products. The sample stored under dry air also shows very weak signals from Na_2CO_3 and water but no decomposition of the $Na_2Fe_2OS_2$ phase, which could come from some low residual humidity during the experiment.

Synthesized by solid-state	**$Na_3Fe_2S_4$ reference**	**Synthesized in dry air**	**Synthesized under Ar**	**Stored in dry air**	**Stored in air (40% RH)**	
		Wavenumber (cm^{-1})				**Assignment**[7]
					239, 249, 272, 283, 294	unidentified
247	250					$Na_3Fe_2S_4$
294	286					
320 (b)		316	312	310		$Na_2Fe_2OS_2$
	325					$Na_3Fe_2S_4$
		348	339	340		$Na_2Fe_2OS_2$
356	347					$Na_3Fe_2S_4$
					358	unidentified
365	365					$Na_3Fe_2S_4$
383 (w)	380 (w)					
430		452	458	456		$Na_2Fe_2OS_2$
					476	unidentified
486		493	486	488		$Na_2Fe_2OS_2$
	525 (b)					$Na_3Fe_2S_4$
		629	615	628		$Na_2Fe_2OS_2$
665		656	659	654		
					693-700	Na_2CO_3
794		838	820	826		$Na_2Fe_2OS_2$
877 (w)				876	877	Na_2CO_3
962 (w)		942	950	969		$Na_2Fe_2OS_2$
	994 (w)					unidentified
1126 (w)		1110	1079-1108	1111	1111	$Na_2Fe_2OS_2$
				1416	1410-1419	Na_2CO_3
				1577	1583	carbonate
					3451	-OH
				3630	3643	H_2O

b (broad), w (weak)

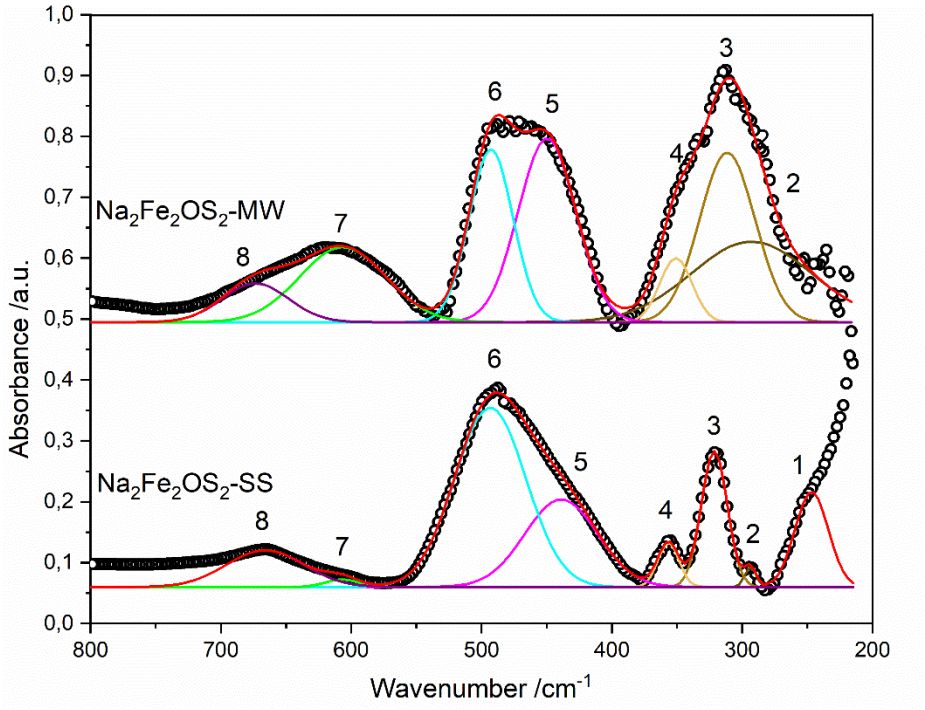

Figure S15. Experimental FTIR spectra of $Na_2Fe_2OS_2$-SS and $Na_2Fe_2OS_2$-MW (black empty circles) along with the resulting fit (red line) using a Gaussian function for each peak (contribution from each peak is shown with other color lines).

Table S8. Result of the peak fitting, using the Gaussian function, of the FTIR spectra of $Na_2Fe_2OS_2$-SS and $Na_2Fe_2OS_2$-MW, where y_0 is the base (in a.u.); x_c, the center (in cm^{-1}); A the area (in a.u.) and FWHM the full width at half maximum (in cm^{-1}) of the peak.*nf refers to "not fitted": these parameters where fixed during the fit in order to avoid divergence.

Peak number	Parameter	$Na_2Fe_2OS_2$-SS		$Na_2Fe_2OS_2$-MW	
		Value	Standard Error	Value	Standard Error
All	y_0	0.06	nf*	0.04	nf
1	x_c	247	nf	/	/
1	A	5	nf	/	/
1	FWHM	30	nf	/	/
2	x_c	294	2	292	2
2	A	0.35	nf	10.2	0.3
2	FWHM	10	nf	109	3
3	x_c	321.4	0.3	310	2
3	A	5.6	0.2	10	0.5
3	FWHM	23.4	0.8	50	2
4	x_c	356.5	0.8	350	2
4	A	1.5	0.1	2.1	0.4
4	FWHM	19	2	29	3
5	x_c	439	6	449	2
5	A	10	3	11.1	0.7
5	FWHM	66	7	52	3
6	x_c	493	3	492	1
6	A	20	3	8	1
6	FWHM	64	3	40	2
7	x_c	607	nf	606	2
7	A	0.4	nf	6.8	0.3
7	FWHM	30	nf	78	4
8	x_c	666	nf	673	nf
8	A	4.5	nf	2.7	0.3
8	FWHM	70	nf	60	nf

3. Study of electrochemical properties

3.1. Rate capability of $Na_2Fe_2OS_2$

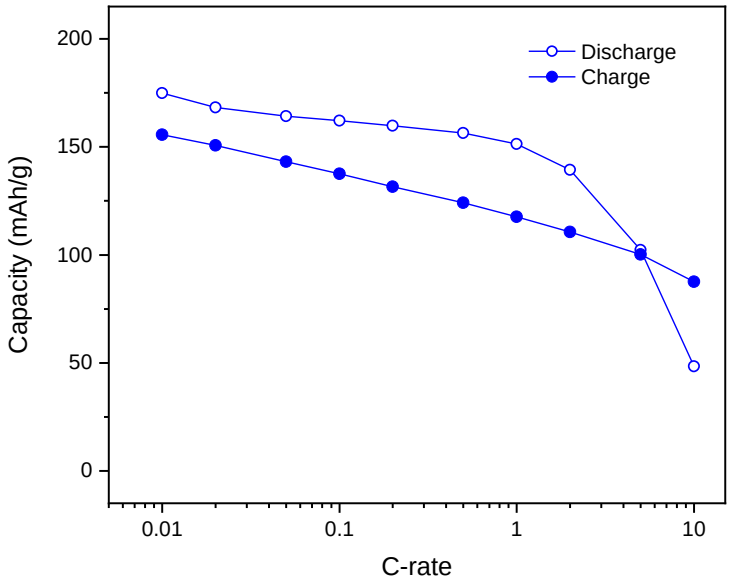

Figure S16. Signature curve of the rate capability of $Na_2Fe_2OS_2$ measured in a 3 electrode cell using metallic Na as a counter and reference electrodes and 1M $NaPF_6$ in EC:DMC + 2 % FEC as an electrolyte. The rate capability was measured after 3 initial cycles at C/10 between 1.5 and 3 V by applying decreasing values of C-rate from 10C to C/100 with 10 h rest periods between each rate step. For more details on this method, see M. Doyle et al.[7]

3.2. Reversibility of phase transition to $Na_{1.7}Fe_2OS_2$

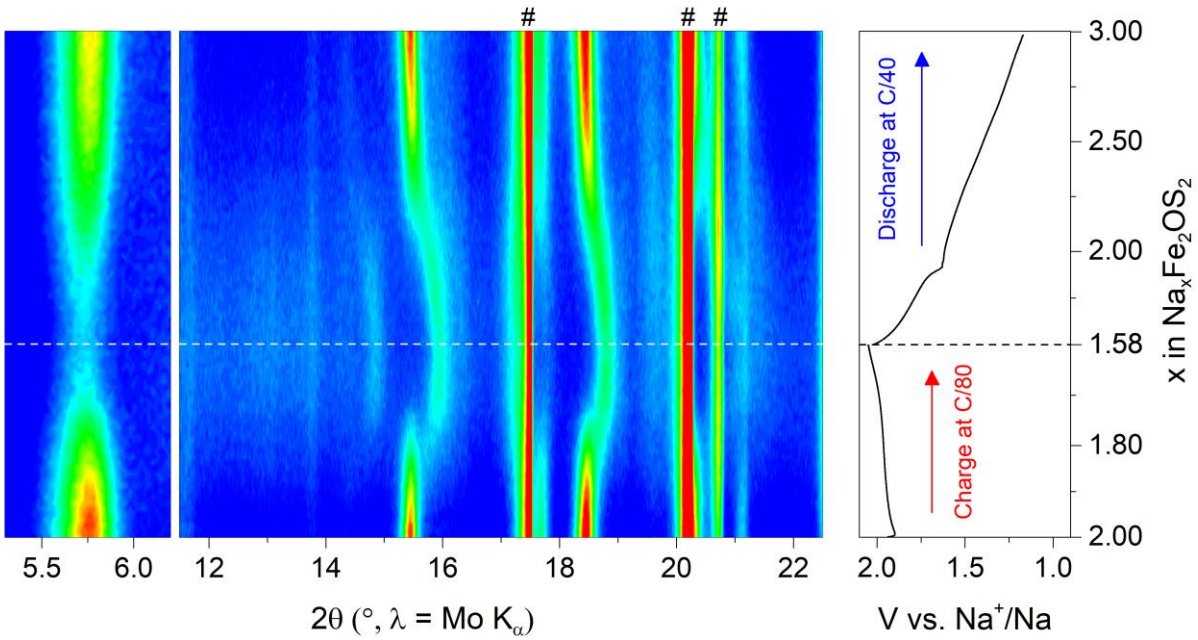

Figure S17. *In situ* XRD measurement limited to 2.05 V on charge then discharged, showing the reversibility of the structural transition between the pristine $Na_2Fe_2OS_2$ structure and the intermediate structure of $Na_{1.7}Fe_2OS_2$. It takes more capacity on discharge to recover the same cell parameters as in the pristine material, although it is not clear if the discharged sample contains more Na than the pristine one. Peaks from the *in situ* setup (Be/Al) are indicated by #. A faster rate on discharge than on charge was used in the interest of time.

3.3. Structure determination of the partially charged sample $Na_{1.7}Fe_2OS_2$

First, identification of impurities in the sample was performed. We found some Fe (~3.6(1) w%), Fe_3O_4 (~1.9(2) w%) and ZrO_2 (~1.1(1) w%) to be present in small quantity in our sample. These phases were then refined along with $Na_{1.7}Fe_2OS_2$ in all of the following analysis. Then, an attempt for Rietveld refinement was performed using a similar structural model with 15 % Na vacancies corresponding to the composition $Na_{1.7}Fe_2OS_2$. This model did not fit our data properly (χ^2 = 30.3 and the residual electron density was high with [ρ_{min} ; ρ_{max}] = [-19.7 ; 3.04] $e^-/Å^3$, Figure S19).

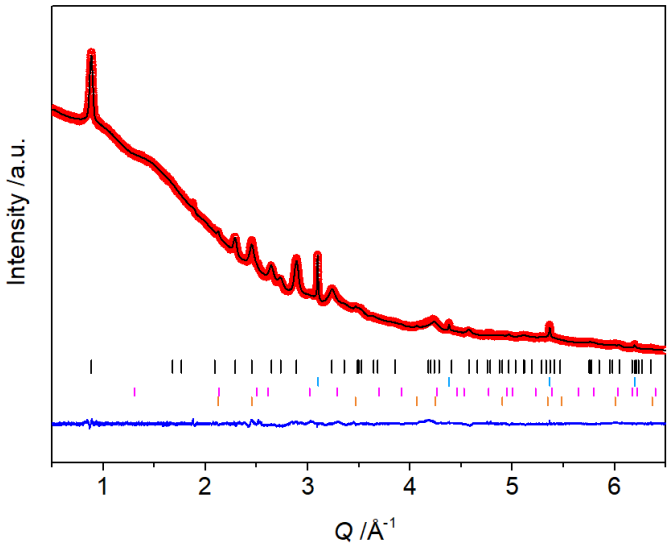

Figure S18. Le Bail fit of the $Na_{1.7}Fe_2OS_2$ phase in the *I*4/*mmm* space group with lattice parameters *a* = 3.8814(6) Å and *c* = 14.260(3) Å (Diamond light source, I11 beam line) with I_{obs} (red dots), I_{calc} (black line), I_{obs}-I_{calc} (blue line), and Bragg reflections (black tick marks for $Na_2Fe_2OS_2$, blue tick marks for Fe, pink tick marks for Fe_3O_4 and orange tick marks for ZrO_2).

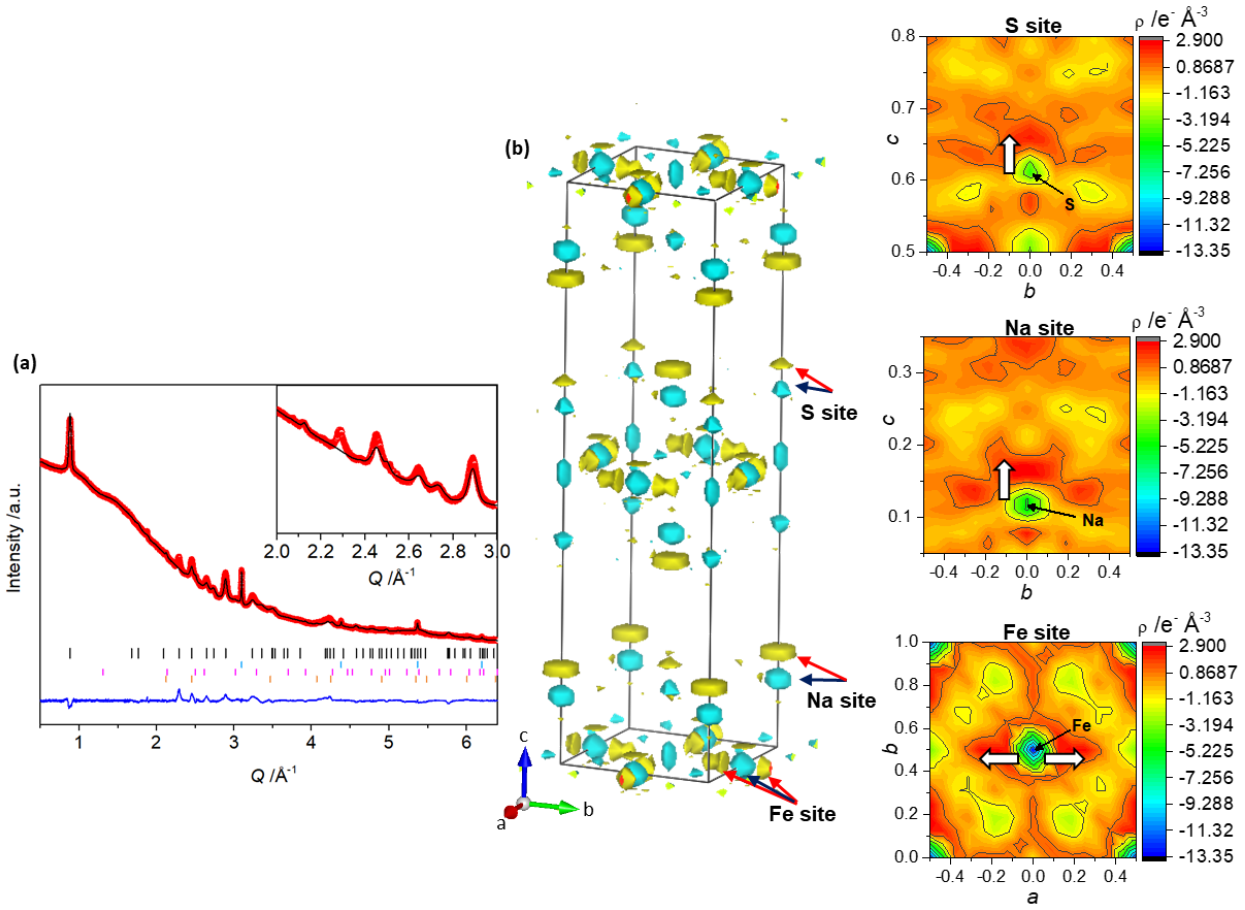

Figure S19. (a) Rietveld refinement of the synchrotron X-ray diffraction pattern of $Na_{1.7}Fe_2OS_2$ using the model obtained for the pristine sample (Table S6, with *sof* of Na fixed to 0.85) (Diamond light source, I11 beam line) with I_{obs} (red dots), I_{calc} (black line), I_{obs}-I_{calc} (blue line), and Bragg reflections (black tick marks for $Na_2Fe_2OS_2$, blue tick marks for Fe, pink tick marks for Fe_3O_4 and orange tick marks for ZrO_2). (b) Fourier difference map of the refinement showing some positive (yellow, and red arrow) and negative (light blue and blue arrow) residual electronic density.

The Fourier difference maps highlighted regions where electron density should be removed (blue arrow on Figure S19b) or added (red arrow). In particular, the S and Na sites seemed to be displaced toward each other, whereas the Fe site appeared to be displaced in the (*ac*) plane on a 16*n* (x, 0.5, z) position. The displacement required for each atom are highlighted by white arrows in the 2D Fourier difference map on Figure S19b. These positions were then refined (by dividing the occupancy of the Fe atom by four due to the change in multiplicity on this new site), first independently, then together. This enabled to improve the quality of the fit (χ^2 = 22.0 and [ρ_{min} ; ρ_{max}] = [-1.42 ; 2.91] $e^-/Å^3$), although not satisfyingly (Figure S20). The Fourier difference

map still showed a negative residual density around the Fe site (blue arrows on Figure S20, -1.6 $e^-/Å^3$), whereas positive around both the Na and S sites (red arrows, +2.98 and 2.36 $e^-/Å^3$, respectively).

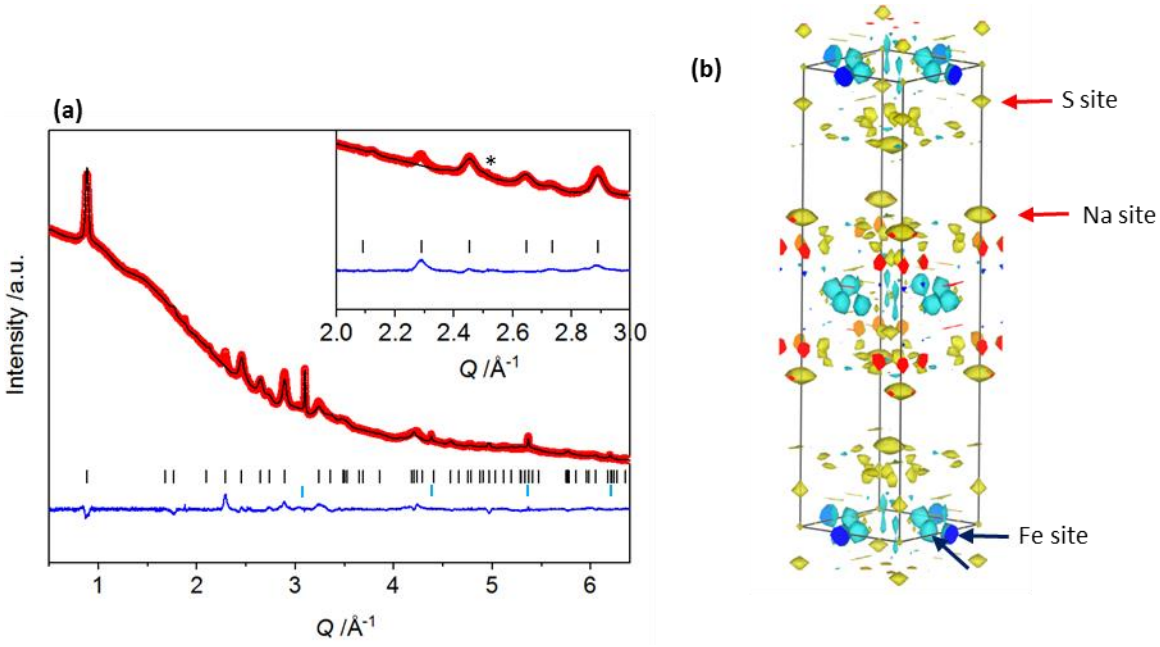

Figure S20. (a) Rietveld refinement of the synchrotron X-ray diffraction pattern of $Na_{1.7}Fe_2OS_2$ by refining the S, Na and Fe (0,y,0) position from the model obtained for the pristine sample (Table S6, with *sof* of Na fixed to 0.85) (Diamond light source, I11 beam line) with I_{obs} (red dots), I_{calc} (black line), I_{obs}-I_{calc} (blue line), and Bragg reflections (black tick marks for $Na_2Fe_2OS_2$ and blue tick marks for Fe, and * for Fe_3O_4). (b) Fourier difference map of the refinement showing some positive (yellow, and red arrow) and negative (light blue and blue arrow) residual electronic density.

The S site was split onto two positions along the z axis, the positions and occupancy and isotropic displacement parameters were refined first independently, then together, by constraining the sum of the *sof* to be equal to 1. This did not improve the fit of the pattern (χ^2 = 22.2). When *sof* of each atom was refined independently and successively for Fe, S and Na, the fit improved considerably (χ^2 = 14.7, [ρ_{min} ; ρ_{max}] = [-1.55 ; 2.87] $e^-/Å^3$ and the modelled peak at Q = 2.3 $Å^{-1}$ started to show some intensity). In accordance to the observed residual density in the Fourier difference map in Figure S20b, *sof* of Fe, Na and S refined to 0.75, 0.8 and 1.1 respectively, which is iron deficient compared to the expected composition $Na_{1.7}Fe_2OS_2$.

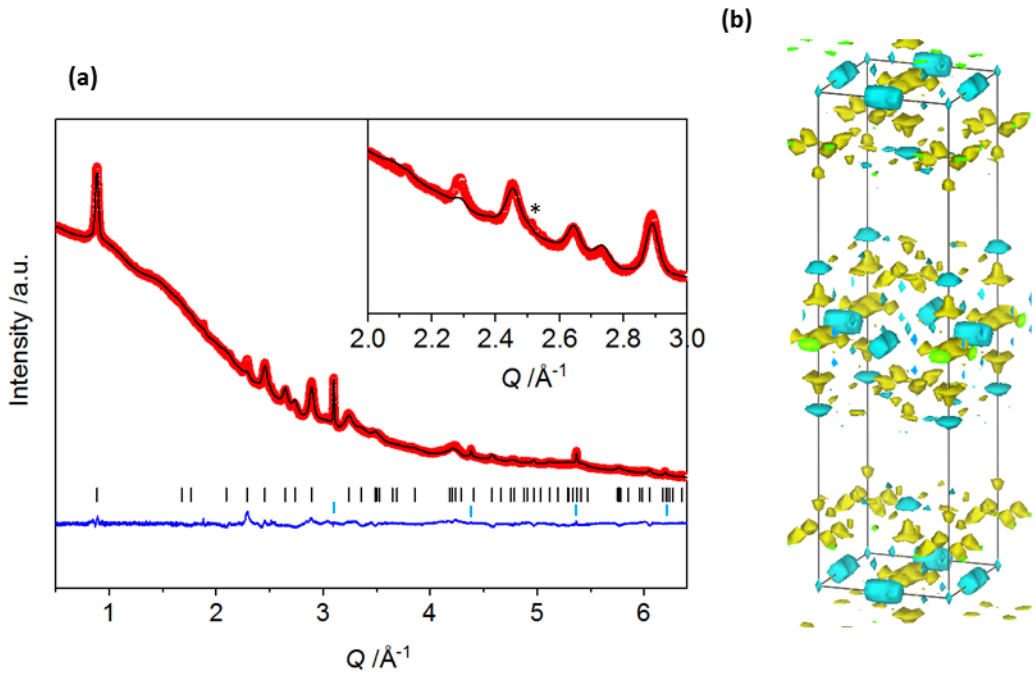

Figure S21. (a) Rietveld refinement of the synchrotron X-ray diffraction pattern of $Na_{1.7}Fe_2OS_2$ by refining the S, Na and Fe (x,0.5,0) positions and *sof* from the model initially obtained for the pristine sample (Table S6) (Diamond light source, I11 beam line) with I_{obs} (red dots), I_{calc} (black line), I_{obs}-I_{calc} (blue line), and Bragg reflections (black tick marks for $Na_2Fe_2OS_2$ and blue tick marks for Fe, and * for Fe_3O_4). (b) Fourier difference map of the refinement showing some positive (yellow) and negative (light blue) residual electronic density.

In order to account for the remaining Fe and Na atoms, some Fe anti site defect onto the Na site was considered as well as some Na anti site defect onto the Fe site. First, the sum of the *sof* of Fe, Na and S were constrained to be equal to 1, 0.85 and 1, respectively. Then the *sof* of Na and S atoms were refined by keeping that of Fe and O fixed to 1. Positions and displacement parameters were then refined independently before refining all parameters together. The site splitting of S was maintained as a marked anisotropy of its displacement parameters was found along the z axis when it was only refined as one site. This yielded the final model (Figure 6c in the main text, χ^2 = 9.51) with refined composition $Na_{1.6(1)}Fe_{2.0(1)}OS_{1.98(10)}$. The outcome of the refinement is presented in Table S9 and Table S10.

Table S9. Result of the Rietveld refinement of the partially charged phase $Na_{1.7}Fe_2OS_2$ ($Na_{1.7}Fe_2OS_2$-PC).

Identifier	**$Na_{1.7}Fe_2OS_2$-PC**
Radiation	**SXRD**
Empirical formula	$Na_{1.6(1)}Fe_{2.0(1)}OS_{1.98(10)}$
Formula weight (g·mol^{-1})	228.6
Space group	*I*4/*mmm*
Z	2
Density (g·cm^{-3})	3.548
Temperature (K)	298
Wavelength (Å)	0.82448
d spacing range (Å)	0.5726 – 22.6275
2θ (°) range	2.0840 - 92.1120
2θ (°) step	0.004
No. of reflections	240
No. of refined parameters	16 (profile), 20 (atomic)
***a* (Å)**	3.8814(7)
***c* (Å)**	14.258(3)
Volume (Å^3)	214.8(1)
R_p	30.1
R_{wp}	20.4
R_{exp}	6.70
R_{Bragg}	13.3
χ^2	9.1
$\rho_{min./max.}$ **residuals (e$^-$·Å^{-3})**	[-11.4 / +3.6]

Table S10. Atomic positions, isotropic (B_{iso}) atomic displacement parameters, and site occupancy factor (*sof*) for the partially charged phase $Na_{1.7}Fe_2OS_2$ ($Na_{1.7}Fe_2OS_2$-PC) obtained from the Rietveld fit of SXRD data.

Site	**Wyckoff position**	**x**	**y**	**z**	***sof***	**B_{iso} (Å^2)**
Na	4*e*	0	0	0.183(5)	0.41(3)	1.0(1)
Fe_i	4*e*	0	0	0.157(1)	0.38(4)	0.6(3)
Fe	16*n*	0.102(4)	0.5	0.024(2)	0.16(3)	0.6(3)
Na_i	16*n*	0.102(4)	0.5	0.024(2)	0.10(3)	1.3(3)
S	4*e*	0	0	0.378(3)	0.56(4)	1.5(5)
S	4*e*	0	0	0.349(3)	0.43(6)	1.5(5)
O	2*a*	0	0	0	1	0.6(3)

Table S11. Selected interatomic distances and bond valence sums (BVS*) for the partially charged phase $Na_{1.7}Fe_2OS_2$ ($Na_{1.7}Fe_2OS_2$-PC).

Atom	Distance around atom (Å)			Coordination	BVS*
Na	Na	S	2.878(3) x4	6	1.63(1)
	Na	S	2.782(2) x4		
	Na	S	2.792(9)		
	Na	S	2.377(9)		
	Na	O	2.602(8)		
Fe_i	Fe_i	S	2.791(9) x4	6	1.08(2)
	Fe_i	S	2.746(3) x4		
	Fe_i	S	2.739(6)		
	Fe_i	S	3.154(6)		
	Fe_i	O	2.240(3)		
Fe / Na_i	Fe	S	2.717(4)	6	Fe: 2.28(7)
	Fe	S	2.080(5)		
	Fe	S	3.127(5)		
	Fe	S	2.592(5)		
	Fe	S	2.951(4)		
	Fe	S	2.377(5)		
	Fe	S	2.935(5)		
	Fe	S	3.416(6)		
	Fe	O	2.010(7) x2		

3.4. Local structure around Fe atoms by EXAFS analysis

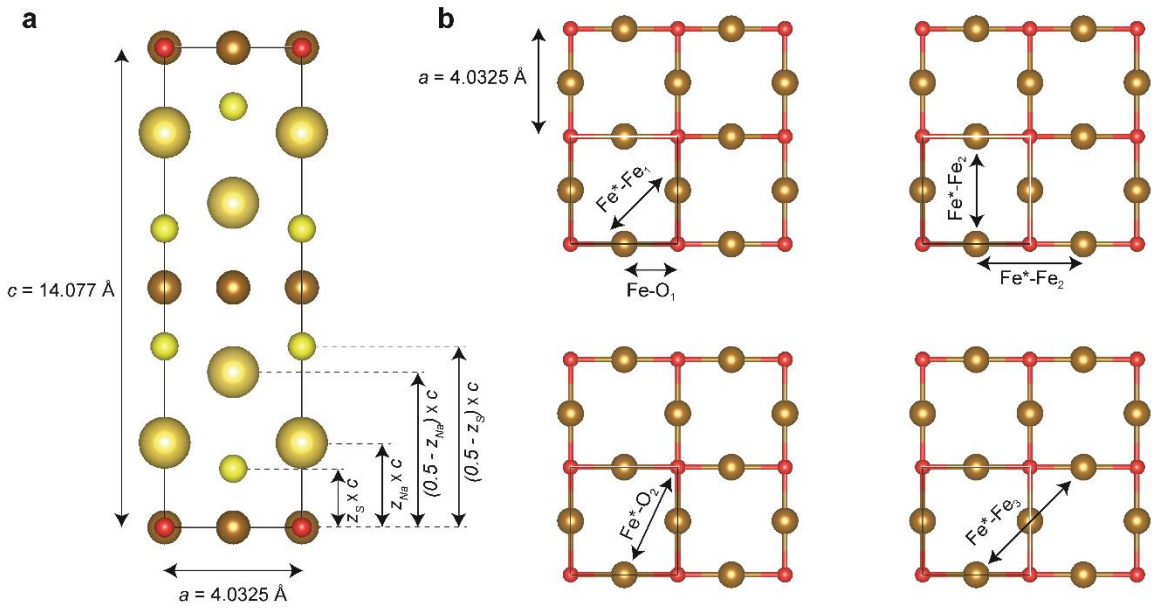

Figure S22. Geometrical parametrization of scattering paths for EXAFS analysis of the crystalline $Na_2Fe_2OS_2$ phase, based on lattice parameters and atomic position extracted from diffraction data. (a) Height of different atoms along the *c*-axis and (b) distances of Fe and O atoms in the *ab* plane. The geometrical formula used for individual scattering paths are listed in Table S12.

Table S12. List of scattering paths used to model the EXAFS data of the crystalline $Na_2Fe_2OS_2$ phase and their geometrical parametrization based on crystallographic parameters.

Scattering path	Type	Parametrization
Fe*-O_1-Fe*	single scattering	$\frac{a}{2}$
Fe*-S_1-Fe*	single scattering	$\sqrt{\left(\frac{a}{2}\right)^2 + (z_s \times c)^2}$
Fe*-Fe_1-Fe*	single scattering	$\frac{a\sqrt{2}}{2}$
Fe*-Na_1-Fe*	single scattering	$\sqrt{\left(\frac{a}{2}\right)^2 + (z_{Na} \times c)^2}$
Fe*-Fe_2-Fe*	single scattering	a
Fe*-O_1-Fe_2-Fe*	multiple scattering	
Fe*-O_1-Fe_2-O_1-Fe*	multiple scattering	
Fe*-O_2-Fe*	single scattering	$\frac{a\sqrt{5}}{2}$
Fe*-S_2-Fe*	single scattering	$\sqrt{\left(\frac{a\sqrt{5}}{2}\right)^2 + (z_s \times c)^2}$
Fe*-Na_2-Fe*	single scattering	$\sqrt{\left(\frac{a\sqrt{5}}{2}\right)^2 + (z_{Na} \times c)^2}$
Fe*-Na_3-Fe*	single scattering	$\sqrt{\left(\frac{a}{2}\right)^2 + ((0.5 - z_{Na}) \times c)^2}$
Fe*-S_3-Fe*	single scattering	$\sqrt{\left(\frac{a}{2}\right)^2 + ((0.5 - z_s) \times c)^2}$
Fe*-Fe_3-Fe*	single scattering	$a\sqrt{2}$
Fe*-Fe_1-Fe_1-Fe*	multiple scattering	
Fe*-Fe_1-Fe_3-Fe*	multiple scattering	
Fe*-Fe_1-Fe*-Fe_1-Fe*	multiple scattering	
Fe*-Fe_1-Fe_3-Fe_1-Fe*	multiple scattering	

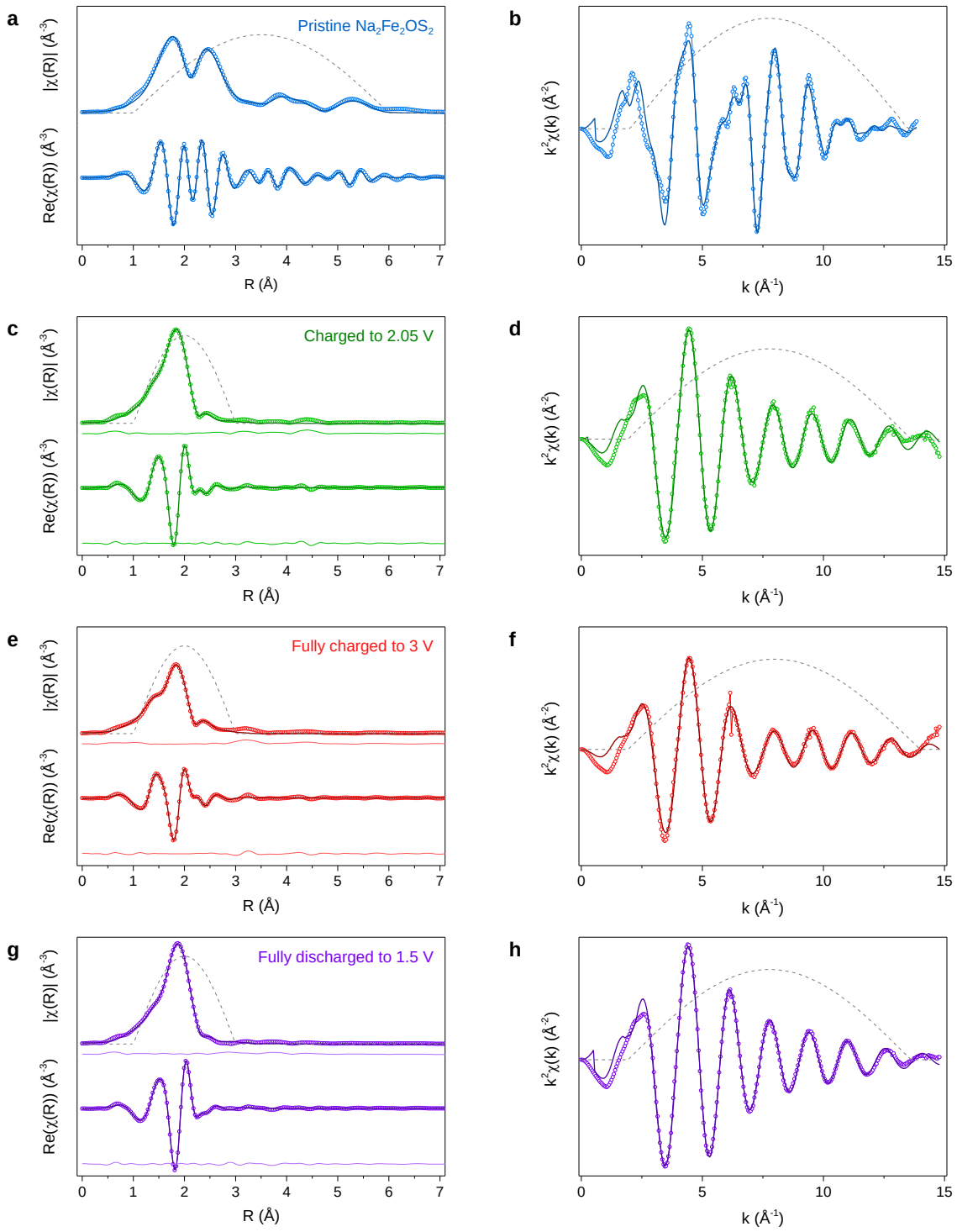

Figure S23. Result of fitting EXAFS data for the pristine (a, b), charged to 2.05 V (c, d), fully charged to 3 V (e, f) and fully discharged to 1.5 V (g, h) samples. The data are weighted by k^2 in all the graphs but the fitting was carried on with data weighted by k, k^2 and k^3. The fits of the magnitude and real parts of the Fourier transform (a, c e and g) are shown, with the corresponding windows and the residual line (light colored line below data). The fit of the data in k-space (b, d, f and h) is also shown with the corresponding window used for the Fourier transform. Experimental data is plotted with circle markers, the fit as a full line, and the sine windows used as grey dashed lines.

Table S13: Local structural parameters obtained from fitting the extended X-ray absorption fine structure for the pristine $Na_2Fe_2OS_2$ and cycled samples (partially charged, fully charged and fully discharged). ΔE_0 is the shift from the edge energy chosen during the background subtraction, S_0^2 is the amplitude reduction factor, σ^2 is the Debye-Waller factor and R is the half-path length of the scattering paths (equivalent to the bond distance between atoms for linear scattering paths). The k-range and R-range on which the fit is performed is indicated for each sample, with the number of independent parameter (N_{ind}) according to the Nyquist criterion, the number of variables used (Nvar) and the R-factor for the final fit. The fit was done on k, k^2 and k^3-weighted data at the same time.

Scattering paths	Multiplicity	ΔE_0 (eV)	S_0^2	σ^2 (10^{-3} Å^2)	Half-path length (Å)
Pristine ($Na_2Fe_2OS_2$)[a]			k = 2.5-12.5 Å^{-1}, R = 1-6 Å, N_{ind} = 30, N_{var} = 15, *R-factor = 1.62 %*		
Fe*-O_1-Fe*	2	1.2(7)	0.87(11)	8(2)[a]	2.01625(5)[b]
Fe*-S_1-Fe*	4			9(1)	2.615(10)
Fe*-Fe_1-Fe*	4			8(1)	2.85141(7)[b]
Fe*-Na_1-Fe*	4			9(3)	3.20(2)
Fe*-Fe_2-Fe* Fe*-O-Fe_2-Fe*[b] Fe*-O-Fe_2-O-Fe*[b]	4 4 2			10(2)	4.03250(10)[b]
Fe*-O_2-Fe*	4			11(7)	4.50847(11)[b]
Fe*-S_2-Fe*	8			16(4)	4.806(5)
Fe*-Na_2-Fe*	4			13(6)	4.979(15)
Fe*-Na_3-Fe*	8			13(6)	5.148(15)
Fe*-S_3-Fe*	4			4(3)	5.739(5)
Fe*-Fe_3-Fe* Fe*-Fe_1-Fe_1-Fe* Fe*-Fe_1-Fe_3-Fe* Fe*-Fe_1-Fe*-Fe_1-Fe* Fe*-Fe_1-Fe_3-Fe_1-Fe*	4 4 8 4 4			14(4)	5.70282(14)[b]
Fe*-S-Fe* (amorphous phase)	4	1.2(7)	0.87(11)	9(1)	2.290(6)
Charged to 2.05 V ($Na_{1.7}Fe_2OS_2$)			k = 3-12.6 Å^{-1}, R = 1-3 Å, N_{ind} = 12, N_{var} = 8, R-factor = 0.06 %		
Fe*-O-Fe*	2	0.3(4)	0.340(10)	7.9(1.1)	1.917(8)
Fe*-S-Fe*	4			4.0(3)	2.268(2)
Fe*-Fe-Fe*[c]	4			24(2)[c]	2.706(10)
Fully charged to 3 V ($Na_{0.5}Fe_2OS_2$)			k = 3-13 Å^{-1}, R = 1-3 Å, N_{ind} = 12, N_{var} = 8, R-factor = 0.09 %		
Fe*-O-Fe*	2	-1.0(4)	0.268(8)	4.8(7)	1.878(6)
Fe*-S-Fe*	4			4.3(3)	2.256(3)
Fe*-Fe-Fe*[c]	4			18(2)[c]	2.700(8)
Fully discharged to 1.5 V ($Na_{1.95}Fe_2OS_2$)			k = 3-12.6 Å^{-1}, R = 1-3 Å, N_{ind} = 12, N_{var} = 8, R-factor = 0.09 %		
Fe*-O-Fe*	2	1.0(6)	0.400(18)	12(2)	1.927(19)
Fe*-S-Fe*	4			4.9(5)	2.296(5)
Fe*-Fe-Fe*[c]	4			28(3)[c]	2.70(3)

[a] The data was fitted considering 40% crystalline phase, and 60% of an amorphous phase. Half-path lengths in the crystalline contribution were constrained according to crystallographic parameters (*a*, *c*, z_S, z_{Na}). Lattice parameters *a* and *c* were fixed to the values of the crystallographic model while z_S, z_{Na}, ΔE_0, S_0^2 and all Debye-Waller factors were refined.

[b] The uncertainties on the distances in the *ab* plane are propagated from the uncertainty on the a lattice parameter obtained from diffraction data, as *a* was fixed in the EXAFS model.

[c] The Fe Fe*-Fe-Fe* scattering paths was included to help fitting the first shell in the amorphous samples but is unlikely to give physical information according to the large Debye-Waller factor.

Calculation of the root mean square (rms) displacement of Fe and S from the adp.

$$U_{ij}(X) = \frac{B_{ij}\,(X)}{8\pi^2}$$

$$rms(X)_{ij} = \sqrt{U_{ij}(X)}$$

$$rms(X)_{Fe-S} = \sqrt{\frac{1 + ((z_{Fe} - z_S)/\,a/2)^2}{\frac{((z_{Fe} - z_S)/\,a/2)^2}{rms(Fe)_{33}} + \frac{1}{rms(Fe)_{11}}}}$$

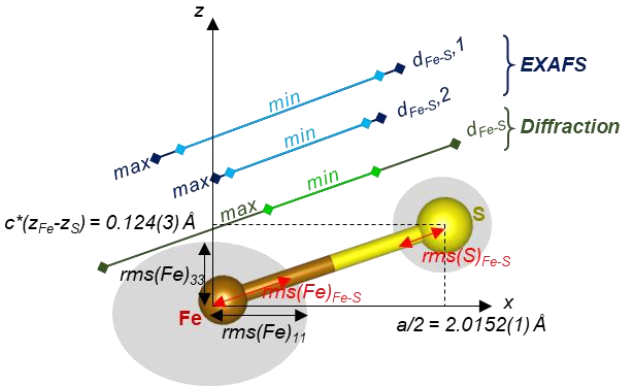

Figure S24. Representation of the minimum and maximum Fe-S distances in $Na_2Fe_2OS_2$-MW determined through the fit of diffraction data and the calculation of the rms displacement of Fe and S from the refined anisotropic tensor matrix U_{ij} and through the fit of the EXAFS data and the calculation of the rms relative displacement from the value of the refined σ^2. Where $rms(X)_{ij}$ is the rms displacement of species X from the anisotropic tensor matrix $U_{ij}(X)$ and $B_{ij}\,(X)$, $rms(X)_{Fe-S}$ is the rms displacement of species X along the Fe-S vector, and z_{Fe} and z_S are the z coordinate of Fe and S respectively.

Table S14. Root mean square displacements of Fe and S along *a*, *c* and Fe-S directions

direction	*a*	*c*	*Fe-S*
rms (Fe) /Å	0.16(7)	0.15(7)	0.16(7)
rms (S) /Å	0.17(8)	0.17(8)	0.17(8)

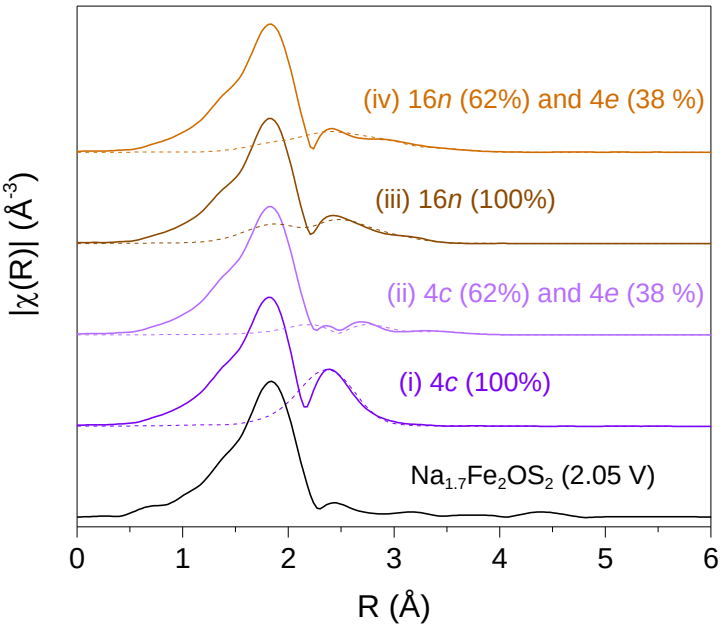

Figure S25. Simulation of EXAFS data to understand the effect of Fe partial occupation of site 4*e* (antisite defects) and Fe displacement from site 4*c* to 16*n* on the intensity of the magnitude of the Fourier transform. The first shell (Fe^{*}-O and Fe^{*}-S) was refined from the experimental data (see Table S13) and was kept constant for all models. Fe^{*}-Fe distances were simulated according to the crystallographic model. Several model were compared: (i) 100% of Fe on the 4*c* site (no displacement and no antisite defect); (ii) 62% of Fe on the 4*c* site (no displacement) and 38% on the 4*e* site (antisite defect); (iii) 100% of Fe on the 16*n* site (displaced and no antisite defect); (iv) 62% of Fe on the 16*n* site (dispalced) and 38% on the 4*e* site (antisite defect). The sum of all Fe^{*}-Fe contributions is plotted as a dashed line and the sum of Fe^{*}-O, Fe^{*}-S and Fe^{*}-Fe contributions is plotted as a full line. The experimental curve for the crystalline $Na_{1.7}Fe_2OS_2$ is plotted in black at the bottom for comparison, showing that the loss of intensity above 2.2 Å can be explained by antisite defects and/or displacement of Fe to a lower symmetry site.

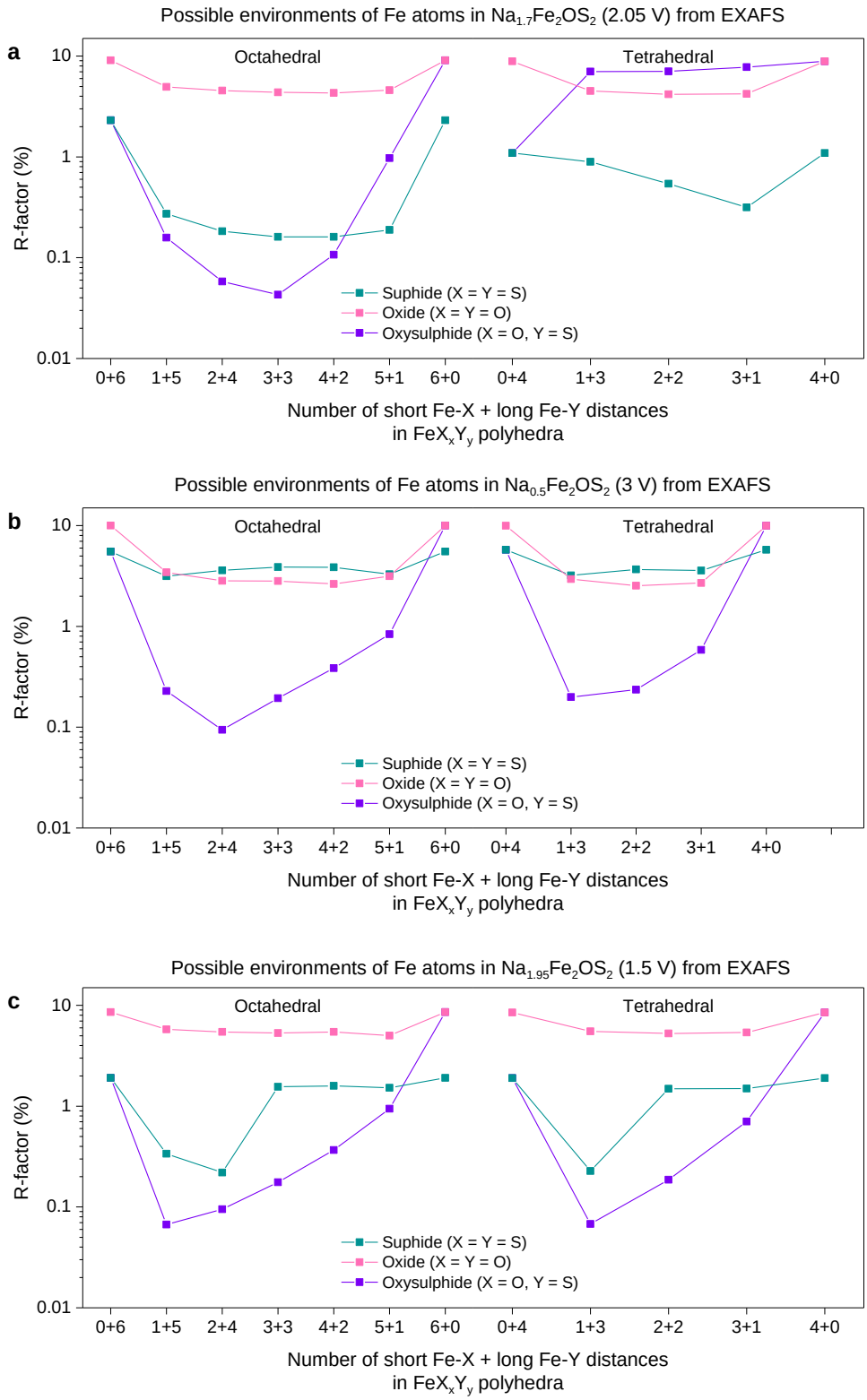

Figure S26. R-factor for different attempts to fit the EXAFS data of $Na_{1.7}Fe_2OS_2$ charged to 2.05 V (a), the amorphous $Na_{0.5}Fe_2OS_2$ phase charged to 3 V (b) and the amorphous $Na_{1.95}Fe_2OS_2$ sample discharged to 1.5 V after a full cycle (c). The data was modelled as an iron oxysulphide, iron sulphide or iron oxide, with multiple combinations of short and long distances in octahedral and tetrahedral coordination environments. Mixed oxygen/sulphur configurations give better results than pure oxide or sulphide configurations. The configuration with four S and two O neighbours, which corresponds to the environment of Fe in the pristine sample, gives good results for all cycled materials.

3.5. Cathode degradation at high voltage and after long cycling.

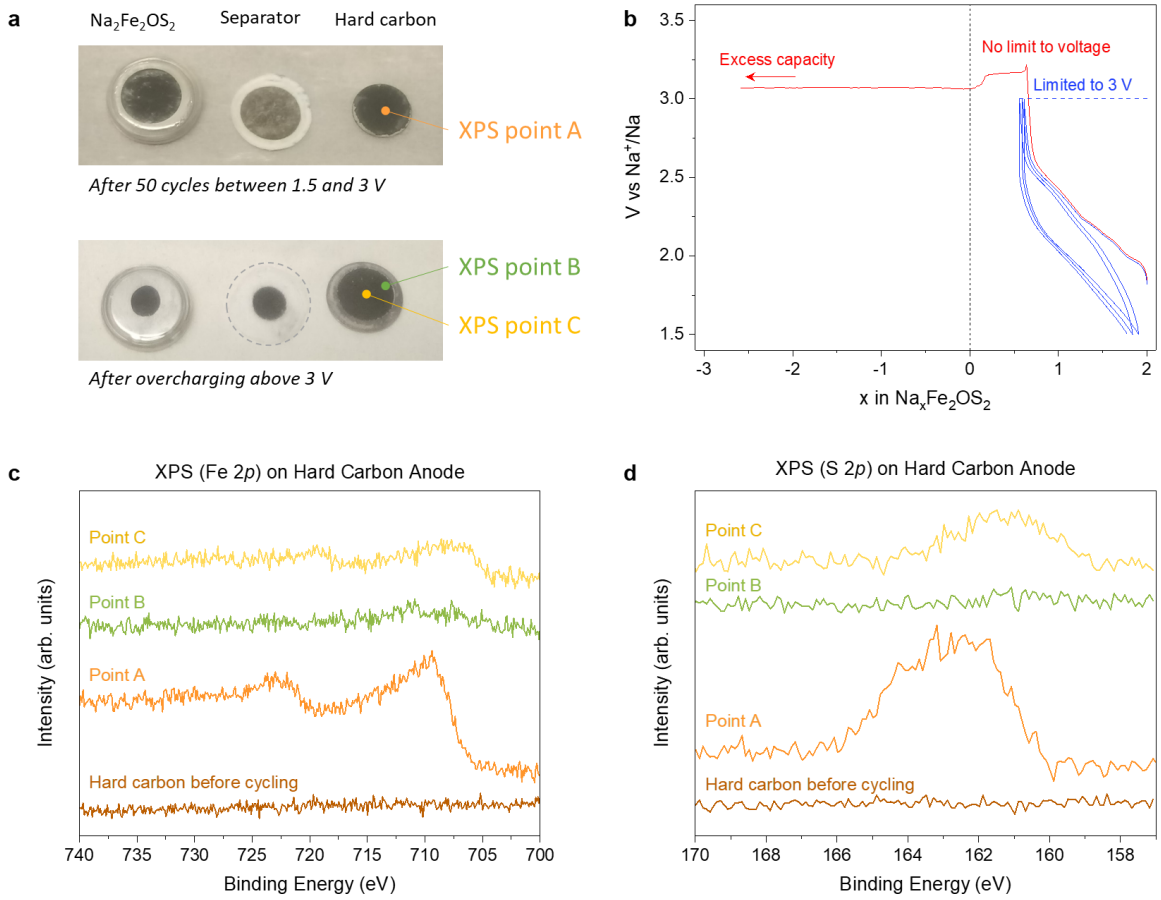

Figure S27. (a) A full cell opened after 50 cycles between 0 and 3 V shows a dark pattern on the separator (center) in front of the $Na_2Fe_2OS_2$ electrode (left) that suggests Fe dissolution. The hard carbon anode (right) was measured by XPS (point A). Another coin cell was disassembled after a single charge above 3 V, also showing a dark pattern on the separator (center, highlighted with dashed circle) that suggests dissolution of the material. The hard carbon counter electrode was measured by XPS at two different points (point B on the side, point C in the center). (b) Electrochemical curve of $Na_2Fe_2OS_2$ when charged above 3 V vs Na^+/Na (red curve), showing a drop in voltage around 3.2 V and an apparent infinite capacity that goes beyond the amount of Na in the material. A reversible charge/discharge curve can be obtained when the voltage is limited to 3 V vs Na^+/Na (blue curve). Both electrochemical curves where measured in 3-electrode cells with Na as a reference electrode and hard carbon as an anode. (c-d) XPS analysis of the hard carbon anode before cycling (pristine, bottom) and after different cycling conditions (point A, B and C in (a)) showing that some Fe and S dissolution happen on the cathode side, eventually depositing on the anode during cycling.

4. Literature search

Reported phases were screened using both Pearson's and ICSD databases by selecting the correct elements for the search of alkali oxysulfide, or by limiting the search to *I*4/*mmm* and *P*4/*mmm* space groups for the search of other anti-RP structures.

Google scholar and Web of Science were both used for the search of cathode materials in the literature by using combinations of appropriate keywords: "oxy sulf*", "cathode*", "ruddlesden popper", "anti", "sodium".

References and citing articles for the paper first reporting $Na_2Fe_2OSe_2$[8] as well as those reporting other materials with the anti Ruddlesden-Popper structure, and the publication reporting the theoretical work on the $Na_{4-c}Li_cAX_4$ (*A* = O and/or S; *X* = I and/or Cl)[9] phases were closely examined and followed in order to avoid any missing information.

Table S 15. Comparison of cathode performances between $LiCoO_2$, candidates as cathode materials for Na-ion batteries, and $Na_2Fe_2OS_2$.

Cathode material	**Capacity (mAh/g)**	**Density (g/cm^3)**	**Volumetric capacity (mAh/cm^3)**
$LiCoO_2$	140	4.8	672
P2-$Na_{2/3}(Fe_{1/2}Mn_{1/2})O_2$	140	4.07	570
$Na_3V_2(PO_4)_2F_3$	110	3.17	349
$Na_2Fe_2OS_2$ (this work)	162	3.41	552

References

[1] J. F. Bérar, P. Lelann, *J. Appl. Crystallogr.* **1991**, *24*, 1.

[2] T. Suzuki-Muresan, P. Deniard, E. Gautron, V. Petříček, S. Jobic, B. Grambow, *J Appl Crystallogr* **2010**, *43*, 1092.

[3] A. G. De La Torre, S. Bruque, M. A. G. Aranda, *J Appl Cryst* **2001**, *34*, 196.

[4] N. Henry, P. Deniard, S. Jobic, R. Brec, C. Fillet, F. Bart, A. Grandjean, O. Pinet, *Journal of Non-Crystalline Solids* **2004**, *333*, 199.

[5] G. W. Brindley, *The London, Edinburgh, and Dublin Philosophical Magazine and Journal of Science* **1945**, *36*, 369.

[6] R. J. Hill, C. J. Howard, *J Appl Cryst* **1987**, *20*, 467.

[7] M. Doyle, J. Newman, J. Reimers, *J. Power Sources*, **1994**, *52*, 211-216.